Deciphering molecular heterogeneity and dynamics of neural stem cells in human hippocampal development, aging, and injury

Junjun Yao[1,2,#], Shaoxing Dai[1,2,#], Ran Zhu[1,2,#], Ju Tan[3,#], Qiancheng Zhao[1,2], Yu Yin[1,2], Jiansen Sun[4], Xuewei Du[1,2], Longjiao Ge[1,2], Jianhua Xu[3], Chunli Hou[3], Nan Li[1,2], Jun Li[2], Weizhi Ji [1,2], Chuhong Zhu[3,*], Runrui Zhang[1,2,*], Tianqing Li[1,2,*]

[1]State Key Laboratory of Primate Biomedical Research; Institute of Primate Translational Medicine, Kunming University of Science and Technology, Kunming, Yunnan 650504, China. [2]Yunnan Key Laboratory of Primate Biomedical Research, Kunming, Yunnan 650504, China. [3]Department of Anatomy, National and Regional Engineering Laboratory of Tissue Engineering, State Key Laboratory of Trauma, Burn and Combined Injury, Key Lab for Biomechanics and Tissue Engineering of Chongqing, Third Military Medical University, Chongqing 400038, China. [4]Zhong-Zhi-Yi-Gu Research Institute, Chongqing 400000, China.

[#]These authors contributed equally to this work.

[*]Correspondence: litq@lpbr.cn (T.L.); zhangrr@lpbr.cn (R.Z.); zhuch99@tmmu.edu.cn (C.Z.)

SUMMARY

While accumulated publications support the existence of neurogenesis in the adult human hippocampus, the homeostasis and developmental potentials of neural stem cells (NSCs) under different contexts remain unclear. Based on our generated single-nucleus atlas of the human hippocampus across neonatal, adult, aging and injury, we dissected the molecular heterogeneity and transcriptional dynamics of human hippocampal NSCs under different contexts. We further identified new specific neurogenic lineage markers that overcome the lack of specificity found in some well-known markers. Based on developmental trajectory and molecular signatures, we found that a subset of NSCs exhibit quiescent properties after birth, and most NSCs become deep quiescence during aging. Furthermore, certain deep quiescent NSCs are re-activated following stroke injury. Together, our findings provide valuable insights into the development, aging, and re-activation of the human hippocampal NSCs, and help to explain why adult hippocampal neurogenesis is infrequently observed in humans.

INTRODUCTION

Continuous learning and memory formation throughout life is driven by developmental and adult neurogenesis. The dentate gyrus (DG), a part of the hippocampus and one of the main neurogenic niches, sustains neurogenesis through the activity of resident neural stem cells (NSCs) (Berg et al., 2019). Although adult neurogenesis in rodents (Dulken et al., 2017; Hochgerner et al., 2018) is well studied, and age-related neurogenesis decline is conserved across species, whether hippocampal neurogenesis persists in the adult human brain has been debated over the years. Finding a conclusive answer to this question is not trivial, as available human brain tissue is rare, and analysis is fraught with technical challenges. Based on marker immunostaining, a few studies found no evidence of neurogenesis in human after adolescence (Cipriani et al., 2018; Franjic et al., 2022; Sorrells et al., 2018), while others detected that human neurogenesis persists in adulthood but declines during aging (Boldrini et al., 2018; Moreno-Jimenez et al., 2019; Terreros-Roncal et al., 2021; Tobin et al., 2019). It is expected that single-cell RNA-sequencing will help resolve the ongoing debate, as this technology is capable of

bypassing the biases associated with traditional methods of immunostaining and quantification. Single cell analysis approaches can also help identify novel cell markers and resolve the dynamics of transcriptional signatures during neurogenesis under different conditions. Leveraging these advantages, several groups performed single-nucleus RNA-seq (snRNA-seq) (Habib et al., 2016) analysis to investigate adult hippocampal neurogenesis in the human brain (Franjic et al., 2022; Wang et al., 2022b; Zhou et al., 2022). Although one study failed to detect evidence of adult neurogenic trajectories in human hippocampal tissues (Franjic et al., 2022), the other two reported the presence of molecular programs consistent with the capacity for the adult human dentate gyrus to generate new granule cells (Wang et al., 2022b; Zhou et al., 2022).

Accumulated publications support the existence of neurogenesis in the adult human hippocampus, but the homeostasis and developmental potentials of NSCs under different contexts remain unclear. Particularly, while actively proliferating in early development, mouse NSCs gradually acquire quiescent properties and transform into quiescent NSCs (qNSCs) with age. Although neurogenesis declines in the mouse aging hippocampus as a consequence of NSC loss and dormancy, qNSCs can be reactivated into active NSCs (aNSCs) that give rise to granule cells (GCs) which integrate into existing neural circuits (Encinas et al., 2011; Obernier and Alvarez-Buylla, 2019). Specifically, ischemic insult in the adult mouse brain has been reported to evoke qNSC to transition into an active state. However, whether these similar mechanisms occur in the human hippocampus is unknown (Llorens-Bobadilla et al., 2015).

To gain insight into why adult hippocampal neurogenesis is challenging to observe in humans, we believe that examining NSCs under varying conditions may be helpful, as they are the source of neurogenesis. Thus, we conducted snRNA-seq analysis on human hippocampal tissue and investigated the heterogeneity and molecular dynamics of hippocampal NSCs across neonatal, adult, aging and stroke-induced injury conditions. Based on comparative analysis of cell types, and developmental trajectories and molecular features of NSCs under different contexts, we found that NSCs, including qNSCs, primed NSCs (pNSCs) and aNSCs, exhibit different molecular features and dynamics across neonatal, adult, aging, and stroke-induced injury conditions. We

observed a subset of NSCs that display quiescent properties after birth, and most NSCs become deep quiescence during aging. Notably, some deep qNSCs can be reactivated to give rise to pNSCs and aNSCs in the stroke-injured adult human hippocampus. In addition, we also found that immature granule cell markers widely used in mice studies, including DCX and PROX1, are non-specifically expressed in human hippocampal GABAergic interneurons. We further identified neuroblast-specific genes *CALM3, NEUROD2, NRN1* and *NRGN* with low/absent expression in human GABAergic interneurons. Together, our findings provide an important resource to understand the development, aging and activation of human postnatal hippocampal NSCs.

RESULTS

Single-nucleus atlas of the human hippocampus across ages and injury

To generate a comprehensive cell atlas of neurogenic lineages in the human hippocampus, we collected 10 donated post-mortem hippocampal tissues. We then dissociated the anterior-mid hippocampus (which has an obvious dentate gyrus structure) and performed 10x genomics single-nucleus RNA-sequencing. We also performed immunostaining for the counterpart side of each hippocampus sample (Figure 1A). The 10 individual samples, divided into four groups according to age and brain health, included neonatal (Day 4 after birth, D4, n=1), adult (31-, 32-year-old, n=2), aging (from 50 to 68-year-old, n=6) and stroke-induced injury (48-year-old, n=1) groups (Figure 1A, Table S1). In total, we sequenced 99,635 single nuclei of which 92,966 nuclei were successfully retained after quality control and filtration. After the removal of cell debris, cell aggregates, and cells with more than 20% of mitochondrial genes transcripts, we analyzed a median of 3001 genes per nucleus. To generate an overview of hippocampal cell types, we pooled single cells from all samples and categorized human hippocampal cells based on classical markers and differentially expressed genes (DEGs) into 16 main populations by Uniform Manifold Approximation and Projection (UMAP) (Figures 1B-2D and S1A-S1C). These included adult astrocyte (adult-AS), AS/qNSC, pNSC, aNSC, neuroblast (NB), granule cell (GC), GABAergic interneuron (GABA-IN), pyramidal neuron (PN), oligodendrocyte progenitor (OPC), oligodendrocyte (OLG), microglia

(MG), endothelial cell (EC), pericyte (Per), relin-expressing Cajal-Retzius cell (CR), and two unidentified cell types (UN1; UN2). Based on the identified populations, the percentage of each cell population in the hippocampus at three different age stages and after stroke-induced injury was quantified and compared. Although some granule cells were lost in the injured hippocampus according to cell percentages, we found that pNSC and aNSC cell numbers decreased markedly with aging but were recovered in the stroke-injured hippocampus (Figure 1E). Overall, cell compositions and proportions varied substantially in neonatal, adult, aging and injured human hippocampus (Figure 1E).

The heterogeneity and molecular features of human hippocampal NSCs

Since hippocampal neurogenesis is controversial in the adult human brain (Boldrini et al., 2018; Cipriani et al., 2018; Franjic et al., 2022; Moreno-Jimenez et al., 2019; Sorrells et al., 2018; Terreros-Roncal et al., 2021; Tobin et al., 2019; Zhong et al., 2020) and the dramatic alteration of related cell types at different statuses was observed (Figure 1E), we mainly focused on the dissection of neural stem cells and neurogenic populations. We first performed a cross-species comparison of our human hippocampal neurogenic populations with the published single cell RNA-seq data from mouse, pig, rhesus macaque and human hippocampus (Franjic et al., 2022; Hochgerner et al., 2018). Neurogenic lineage populations across species were distributed at similar coordinates in the UMAP (Figure 2A). For example, human AS/qNSCs and pNSCs aligned more strongly with astrocytes and radial glia-like cells (RGLs) from other species, and expressed classical RGL genes (Figure 2A). Similarly, human aNSCs and NBs clustered together with other species' neural intermediate progenitor cells (nIPCs) and neuroblasts, respectively (Figure 2A). In addition, neurogenic lineage markers identified in other species were also highly expressed in corresponding populations in our data (Figure 2B). From our snRNA-seq data, the initial clustering (UMAP) was unable to segregate qNSCs from astrocytes in the human hippocampus due to the great similarity of qNSCs and astrocytes (Figure 1B). To elucidate the characteristics of qNSCs in the human hippocampus, astrocytes should be excluded correctly. Therefore, we subclustered the AS/qNSC population for Seurat (Findallmarker) analysis (Figures 2C and 2D).

According to the DEGs and the feature gene expression, three subclusters were identified and annotated as astrocyte (AS), qNSC1, and qNSC2 (Figures 2C and 2D). Next, we used gene set scores analysis to confirm the properties of AS, qNSC1 and qNSC2 according to the global gene expression level (Figures 2E and 2F). Although the RGL gene set hardly distinguishes qNSCs from astrocytes (Figure 2E), analysis of astrocyte feature genes (Clarke et al., 2018; Franjic et al., 2022; Hochgerner et al., 2018; Liddelow et al., 2017; Zamanian et al., 2012; Zhong et al., 2020) revealed that the AS cluster obtained higher astrocyte score than qNSC1 and qNSC2 (Figure 2F). The classical astrocyte markers such as *S100B* and *GFAP* were highly expressed in the AS cluster (Figure 2G). The qNSC1 cluster was characterized by the preferred expression of quiescence NSC gene *HOPX*. Compared with the qNSC1 cluster, the qNSC2 cluster behaved less quiescent since they highly expressed *LPAR1*, neurogenic genes (e.g., *STMN1*, *PROX1*, and *SIRT2*) and oligodendrocyte lineage genes (e.g., *MBP*, *PLP1*, *MOBP*), showing the initial potential of lineage development (Figures 2D and 2G). Compared with astrocyte and quiescent NSCs, pNSCs lowly expressed *ALDH1L1* and *GFAP*, but highly expressed stem cell genes *HOPX*, *VIM*, *SOX2*, *SOX4* and *CCND2* (Figures 1C and 1D). Consistent with their identities, gene ontology (GO) terms of the top 1000 genes in pNSCs included stem cell differentiation, Wnt signaling, neurogenesis, Notch signaling and hippo signaling, indicating that they maintain critical properties of RGLs (Figure 2H). Different from pNSCs, the identified aNSCs highly expressed stem cell and proliferation markers, such as *SOX2, SOX4, SOX11* and *CCND2* (Figures 1C and 1D) and were enriched for GO terms associated with the onset of neuronal fate, such as neuron differentiation, neuron projection morphogenesis, axonogenesis and synapse organization (Figure 2I). Neuroblasts highly expressed *CCND2*, *SOX4*, *STMN2*, *SOX11*, *PROX1* and *NEUROD2*, and started to express several granule cell markers, such as *SYT1* and *SV2B* (Figures 1C and 1D). As expected, qNSC1 and qNSC2 were mainly in the non-cycling G0/G1 phase whereas aNSCs were mainly in the S/G2/M phase of active mitosis, confirming their quiescent and active cell states, respectively (Figure 2J).

Taken together, our findings demonstrate the molecular features of various types of human hippocampal NSCs and their progeny, including qNSCs, pNSCs (RGLs), aNSCs,

and NBs, highlighting the heterogeneity of these cell populations and their unique cell cycle properties.

Novel markers distinguishing various types of NSCs and NBs in the human hippocampus

The lack of validated cell-type specific markers constrains efforts to identify NSCs and their progeny in the human hippocampus. Since single-cell Hierarchical Poisson Factorization (scHPF) (Levitin et al., 2019) could sort out specific genes and seurat analysis (FindAllMarkers) is suitable for searching highly expressed genes, we used the two methods together to narrow the scope of candidate genes, allowing us to identify specific genes that can distinguish qNSCs, pNSC (RGL), aNSC and neuroblast cells from other non-neurogenic cells in the human hippocampus. The combined results from scHPF and FindAllMarkers data showed that *LRRC3B, RHOJ, SLC4A4, GLI3* were specifically expressed in qNSC1 and qNSC2, *CHI3L1* and *EGFR* could be regarded as pNSC marker genes, and *NRGN, NRN1* and *HECW1* as NB marker genes at the transcriptional level (Figures 3A-3C and Table S2). Feature plots revealed that *EGFR* was specific for pNSCs, while *CHI3L1* was also expressed by astrocytes. *NRGN* and *NRN1* but not *HECW1* were specific for NBs (Figure 3C). Notably, several genes enriched in NBs, such as *HECW1*，*STMN2*, *NSG2*, *SNAP25* and *BASP1* (Figure 3C) were also widely distributed in GABAergic interneurons that were validated by high expression of known GABAergic interneuron marker genes, such as *DLX1, GABRG3, CCK, SLC6A11, SLC6A1, GAD1, GAD2, CNR1, GRM1, RELN* and *VIP* (Figures 3C and 3D). When we compared the granule cell lineage and the interneuron population at the whole transcriptome level between our dataset and published mouse (Hochgerner et al., 2018), macaque and human (Franjic et al., 2022) transcriptome datasets, we found high transcriptomic congruence across different datasets (Figure S2A). Specifically, our identified human GABA-INs very highly resembled the well-annotated interneurons in different species (similarity scores > 0.95) (Figure S2A). Based on the validated cell type annotation, we plotted expression of the NB/im-GC highly expressed genes reported by the other studies (Wang et al., 2022b; Zhou et al., 2022) in our identified granule cell

lineage and interneuron population (Figure 3D). Indeed, both the previously reported genes that are regarded as the markers of NB/im-GCs, such as *DCX, PROX1, CALB1, CALB2* (Wang et al., 2022b; Zhou et al., 2022), and here identified genes (*HECW1, STMN2, NSG2, SNAP25* and *BASP1*) were also enriched in neonatal GABAergic interneurons (Figures 3C and 3D). Consistently, these genes were also prominently expressed in the adult interneurons (Figure S2B). These results suggest that identification of newborn neurons using NB/im-GC genes requires the exclusion of the interneuron contamination, as reported by a recent study (Franjic et al., 2022).

To further identify NB/im-GC specific genes absent in interneurons, we mapped the NB/im-GC genes identified by scHPF (top 100) and FindAllMarkers (p-adjust < 0.01) onto the interneuron population (Figure 3E). We selected genes with low or absent expression in the interneuron population (around the coordinate origin) as NB/im-GC specific genes by filtering out genes with high and wide distributions in the interneuron population (Figure 3E). We identified several representative NB/im-GC specific genes, such as *CALM3, TTC9B, NRGN, FXYD7, NRN1, GNG3, TCEAL5, TMSB10* and *NEUROD2* (Figure 3F) and confirmed their specificity in adult and aging samples (Figure S2C).

Overall, our results revealed that most NB/im-GC genes are prominently expressed in human hippocampal interneurons, hence, our newly identified NB marker genes could be used to identify newborn neurons in adult or aging human hippocampus.

The developmental trajectory and molecular cascades of NSCs in neonatal human hippocampus

Based on studies in mice, RGLs acquire quiescence gradually throughout postnatal development and adulthood, and share molecular markers with astrocytes (Alvarez-Buylla and Garcia-Verdugo, 2002; Berg et al., 2019; Garcia et al., 2004; Hochgerner et al., 2018; Ponti et al., 2013; Seri et al., 2001; Steiner et al., 2004). The situation of RGLs in human hippocampus is still unclear. We used RNA-velocity to investigate the developmental potentials of NSCs in the neonatal human hippocampus (Figure 4A). We observed that pNSCs give two developmental directions: one is entering quiescence, and

the other is generating aNSCs. Based on the GO term analysis of the differentially expressed genes comparing qNSC1/2 with pNSCs, it appears that pNSCs are more active (Figure 4B). Since qNSCs originate from RGLs (Figure 4A) but exit out of the cell cycle and development, the pNSC (RGL) population was set as the root of the developmental trajectory to recapitulate the continuum of the neurogenesis process (Figure 4C). According to the developmental trajectory, pNSCs were followed by aNSCs and NBs, and gave rise to two types of neurons (N1 and N2), indicative of ongoing neurogenesis (Figures 4C and S3A and S3B). The N1 and N2 populations had distinct gene expression profiles, which indicates they are subtypes of GCs (Figure S3C). The N1 specifically express *NCKAP5, SGCZ, DCC, FAM19A2,* whereas the N2 specifically express *FLRT2, RIMS2, NKAIN2* and *XKR4* (Figure S3D).

Next, we traced the dynamics of pNSC, aNSC, NB and GC marker genes along with the developmental trajectory (Figure 4D). We found that *HOPX*, *SOX2* and *VIM* expression was preferentially maintained in pNSCs and aNSCs, but decreased upon differentiation. Finally, expressions of NB genes *DCX* and *STMN2* increased along the trajectory and the GC gene *SYT1* reached maximum expression at the end of the trajectory (Figure 4D). To validate the RNA-seq results, we performed immunostaining in the dentate gyrus of D4 neonatal hippocampus. In the granule cell layer (GCL) and hilus, we detected $HOPX^{+}NES^{+}$ RGLs and $Ki67^{+}NES^{+}$ proliferating NSCs (Figure 4E), consistent with previously reported NSC immunostaining in human hippocampus (Sorrells et al., 2018). We also found that PSA-$NCAM^{+}$ neuroblasts located in the GCL as clusters (Figure 4E). These results confirm that both pNSCs (RGLs) and aNSCs maintain their proliferative status and are capable of generating new granule cells in the neonatal human hippocampus.

To understand how gene expression profiles in different cell populations change over the developmental trajectory, we constructed gene expression cascades of neurogenesis-related cell populations (including pNSC, aNSC, NB, and N1/N2) and annotated the DEGs into 4 Clusters (Figure 4F). Cluster 1 population, located at the trajectory start, consists of pNSCs and aNSCs with high expression of *VIM, GFAP, SOX6, GPC6, GPC6, CD44, CHI3L1, TNC, EGFR* and *HOPX.* These genes are mainly related to cell

proliferation, regeneration, angiogenesis and the canonical Wnt signaling pathway (Figure 4F and Table S3). As expected, *HOPX, VIM, CHI3L1* and *TNC* were down-regulated along the presudotime (Figure 4G). Cluster 2 population highly expressed neurogenesis and neuronal differentiation genes, including *NRGN, STMN2* and *NEUROD6*, which reached their expression peak at the middle of the trajectory and represented neuron development (Figures 4F and 4G, Table S3). Cluster 3 and 4 populations, respectively located at the end of two branches, contained neurons that became mature and functional. The genes for the branch 2 (cluster 3) were associated with axon guidance, neurotransmitter secretion, long-term synaptic potentiation and ion transport, such as *SV2B*, *SYT6* and *SYN2*; similarly, the branch1 (cluster 4) genes were associated with neuron projection guidance, dendritic spine organization and excitatory postsynaptic potential, such as *MYT1* and *GIRK2* (Figure 4F). In addition, we also identified transcriptions factors (TFs) that are differentially expressed from pNSC to neurons along with the neurogenesis trajectory in all 4 clusters (Figure S3E. For example, progenitor cell regulation TFs *PBX3, PROX1, GLIS3, RFX4* and *TEAD1* were dominantly enriched in the origin of the trajectory. Conversely, differentiation related TFs *POU6F2, FOXP2, THRB, ETV1, NR4A3, BCL11A, NCALD, LUZP2* and *RARB* were prominently expressed in the middle and the end of the trajectory.

Our findings collectively imply that specific types of human hippocampal NSCs remain in a quiescent state postnatally, serving as a reservoir for potential neurogenesis. Meanwhile, a considerable proportion of NSCs retain their capacity for proliferation and are capable of producing fresh granule cells in the neonatal hippocampus of humans.

Most NSCs become deep quiescence during aging

When we quantified the cell numbers of different types of NSCs and their progeny across neonatal (postnatal day 4), adult (the mean of 31y, 32y) and aging (the mean of 50y, 56y, 60y, 64y-1, 64y-2, 68y) groups, we noted that the ratios of qNSC1 and qNSC2 increased significantly with age, particularly the deep quiescent stem cell qNSC1. Conversely, pNSC and aNSC populations sharply declined from neonatal to adult and aging stages. Meanwhile, the numbers of neuroblasts were comparable in the neonatal and adult brain,

they were markedly reduced in the aging hippocampus (Figures 5A and 5B). Although the number of these neurogenic cells (pNSCs, aNSCs, NBs) in the aged hippocampus is quite low, they still expressed neural stem cell and neuroblast marker genes, including *VIM, PAX6, SOX2, PROX1, NRGN, INPP5F,* and *TERF2IP* (Figure S4A), ruling out that these are contaminated by other neurogenic cell types. These results together showed that pNSCs and aNSCs are present in the neonatal hippocampus, but their numbers significantly decrease with age. This suggests that human neurogenesis experiences a rapid decline after birth. In contrast, neuroblasts have a longer maturation period until adulthood, which is consistent with previous studies (Ayhan et al., 2021; Franjic et al., 2022; Ngwenya et al., 2015; Seki, 2020).

Given the continuity of NSC development and the rarity of neural stem cells in the adult or aged hippocampus, we merged the five cell types qNSC1s, qNSC2s, pNSCs, aNSCs and NBs together as the neurogenic lineage to analyze the transcriptomic alterations during aging. We have observed a significant up-regulation of astrocyte and quiescence genes (*LRRC3B, RHOJ, SLC4A4*) with increasing age, as well as a marked down-regulation of pNSC genes (*HOPX, SOX2, NES, VIM* and *CHI3L1*), aNSC genes (*ASCL1, EOMES* and *MKI67*) and NB genes (*STMN2, DCX*) upon aging (Figure 5C). When we stained hippocampal tissue sections from neonatal D4, 32y and 56y donors (Figures 5D and S4B), we observed that NSC markers HOPX, VIM, NES and CHI3L1, which were widely expressed in the neonatal D4 dentate gyrus, were almost lost in 32y, 50y and 56y dentate gyrus. VIM^+ and NES^+ RGLs were only present around the GCL or in the hilus of the neonatal dentate gyrus (D4); whereas the NB marker PSA-NCAM was expressed in the D4 and 32y dentate gyrus, but not in 50y and 56y hippocampus (Figure 5D). In agreement with previous staining in adult human brain samples (Sorrells et al., 2018), PSA-$NCAM^+$ cells in the GCL of the neonatal and adult dentate gyrus had neuronal morphologies (Figure 5D). Together, our immunostaining analysis is consistent with our snRNA-seq data, confirming that pNSCs and aNSCs experience a significant loss with aging, while neuroblasts are sustained until adulthood in humans.

To explore whether the human hippocampal NSCs are getting more and more quiescent during postnatal development and aging, we compared qNSCs from the

neonatal sample with those from aged samples (Table S4). We observed that cell proliferation and growth inhibition genes (*BRINP1, CABLES1, TENM2, CNTN1*), and stem cell differentiation genes (*RANBP3L, NDRG2*) were up-regulated significantly in qNSC1 during aging. Besides *CABLES1* and *CNTN1,* the oligodendrocyte genes (*MBP, PLP1, MOBP*) were also highly expressed in aging qNSC2 (Figure 5E). In contrast, stem cell and regeneration genes (*LPAR1, TNC, CASC15, SOX2, SOX4, HOPX, VIM*) were down-regulated in qNSC1 and qNSC2 (Figure 5E). The enriched GOs of significantly up-regulated genes in aging qNSC1 and qNSC2 included negative regulation of growth, neuronal stem cell population maintenance, astrocyte differentiation, oligodendrocyte differentiation, aging and amyloid precursor protein catabolic process (Figure 5F and Table S4). Instead, the enriched GOs of significantly down-regulated genes in qNSC1 and qNSC2 were related to nervous system development, neurogenesis, positive regulation of mitotic cell cycle, tissue regeneration, autophagy, generation of neurons, hippo signaling, Wnt signaling pathway and Notch signaling pathway (Figure 5F, Table S4). All these differences between neonatal and aged qNSCs suggest that hippocampal NSCs undergo a transition into a state of deep quiescence and acquire glial properties during aging. In addition, we also compared gene expression of the remaining pNSCs, aNSCs and NBs between neonatal and aged groups, respectively (Figures S5A-S5I). The DEGs and enriched GOs of each cell type also strongly revealed that neurogenesis decline with aging is mainly due to repression of neural stem cell proliferation, deficient autophagy and proteasomal protein catabolic process and increased glial cell differentiation. Overall, the results obtained from both the comparison of the entire neurogenic lineage and the comparison of individual cell types suggest that most NSCs lose their neurogenic potential as a result of entering a state of deep quiescence during aging.

Injury induced activation of qNSCs in the adult hippocampus

The homeostasis of NSCs impacts the dynamics of neurogenesis in response to environmental signals (Chaker et al., 2015; Daynac et al., 2014; Enwere et al., 2004; Katsimpardi et al., 2014) and injury conditions in mice can even reactivate qNSCs into a proliferative state that gives rise to new neurons (Buffo et al., 2008; Llorens-Bobadilla

et al., 2015). In the stroke-afflicted donor (48y), we noted a significant loss of hippocampal granule neurons and interneurons (Figure 1E). Compared to adult donors, genes associated with apoptosis, DNA damage and autophagy were significantly up-regulated in the GCs and GABA-INs of the stroke-injured hippocampus (Figures S6A and S6B). Consistently, we detected evident cell apoptosis by TUNEL assay in the stroke-injured dentate gyrus, but not in other adult or aging samples (Figure S6C). These data validated that injury had occurred in the hippocampus of donors that had suffered from a stroke. Interestingly, in the injured hippocampus, the ratios of the pNSC and aNSC populations in the neurogenic lineage reached up to 35% (977/2722) and 37.6% (1024/2722), comparable to ratios in the neonatal group and significantly higher than the adult and aging groups. Correspondingly, the ratios of qNSC populations qNSC1 (16.0%, 435/2722) and qNSC2 (7.6%, 207/2722) in the neurogenic lineage evidently decreased in the injury group compared with adult and aged groups (Figures 6A and 6B). These results indicated that qNSCs may be reactivated upon injury and give rise to pNSC and aNSC populations. However, we only observed 79 cells in the neuroblast population that highly expressed neuroblast marker genes *PROX1, SEMA3C, TACC2, INPP5F,* and *TERF2IP* (Figure S4A). We speculate that because the patient died within two days after the stroke, there was little time for the activated NSCs to generate more neuroblasts.

When we analyzed gene expression of neurogenic lineage (pooled qNSC1s, qNSC2s, pNSCs, aNSCs and NBs together) in the neonatal, adult, aging and stroke-injured hippocampus by bubble plot, we found that *VIM*, *NES, CHI3L1* and *SOX10* were up-regulated in the injury group compared with adult and aging groups (Figure 6C). The expression of *VIM* and *SOX10* was even higher than in the neonatal group, indicative of prominent gliosis. Previous studies in mice reported that NSCs and astrocytes become activated after stroke around the injured area. Such activated NSCs which could generate newborn neurons together with reactive astrocyte-formed glial scarring may contribute to brain repair (Benner et al., 2013; Faiz et al., 2015; Li et al., 2010). Since activated NSCs and reactive astrocytes share similar transcriptional properties but have distinct morphology, we performed immunostaining of NES/KI67, NES/VIM and NES/CHI3L1 in the stroke-injured dentate gyrus. We detected a few $NES^{+}KI67^{+}$, $NES^{+}VIM^{+}$ and

$NES^+CHI3L1^+$ active NSCs that had radial glia morphology with apical processes (Figure 6D), appearing similar to D4 NES^+ RGLs (Figure 4E). However, we could not detect these active NSCs in any other adult sample (32y, 50y, 56y) (Figure 5D). These results together with the decline of neurogenesis in the aging group suggest that some quiescent NSCs in the adult and aging human hippocampus can be reactivated and give rise to active NSCs upon stroke-induced injury.

However, $VIM^+CHI3L1^+$ reactive astrocytes with an irregular contour or star-shape morphology were widely observed in the injured hippocampus (Figure S6D), reminding us that the pNSC and aNSC populations from the initial UMAP clustering may contain reactive astrocytes. To distinguish activated NSCs (pNSCs and aNSCs) from reactive astrocytes, we integrated neonatal pNSCs and aNSCs with injury samples, and then applied neonatal pNSC and aNSC as cell prototypes to identify pNSCs and aNSCs in the injury sample. We increased cluster resolution and obtained eight subclusters with distinct gene expression profiles (Figures 6E and S7A). When we compared the fraction of each subcluster in neonatal and injury samples, we found subclusters 0, 1 and 3 were predominant in the neonatal sample, and subclusters 2 and 4 were predominant in injury sample (Figure S7B). The results of Gene set score analysis also showed that subclusters 0, 1 and 3 maintained higher RGL potential than subcluster 4, and subcluster 2 had more evident reactive astrocyte properties than subclusters 0, 1 and 3 (Figure 6F). Consistently, RGL specific genes (*VIM*, *HOPX, LPAR1* and *SOX2*) were significantly expressed in subcluster 0, 1 and 3. The neurogenic genes (*STMN1, DCX* and *SIRT2*) were mainly expressed in subcluster 0. The reactive astrocyte marker (*OSMR, TIMP1* and *LGALS3*) were mainly expressed in subcluster2 (Figure S7C). Therefore, cells in subcluster 0 were speculated as pure aNSCs, subclusters 1 and 3 were pNSC in the stroke-injured hippocampus, and cells in subcluster 2 were reactive astrocytes. Since the features of other small subclusters were not clear, they were excluded from the developmental trajectory analysis.

To reconstruct the injury-induced activation trajectory of qNSCs and explore their developmental potential, we included qNSC1, qNSC2, pNSC, aNSC and NB as neurogenic lineage for further analysis. In agreement with previous studies of adult

neurogenesis (Artegiani et al., 2017; Dulken et al., 2017), the trajectory originated from qNSC1, qNSC2, and progressed to pNSCs, and then to aNSCs or NBs (Figure 6G). Based on this trajectory, *HOPX* and *PAX6* were mainly expressed where qNSCs were located, then *VIM, CD44, TNC* and *CHI3L1* reached their expression peaks in the middle of the trajectory where pNSCs located, following by *SOX2, CKAP5, RANGAP1* genes in aNSCs and *STMN2* gene in NBs (Figure S7D). The trajectory and gene expression together support that qNSCs can be activated to become pNSCs and aNSCs. Since the patient did not live long after the stroke, we attempted to predict the developmental potential of NSC lineages by analyzing the gene expression cascade along with the pseudotime. According to the gene expression cascade，DEGs corresponding to 4 clusters were identified (Figure 6H). *TNC, SOX2, LPAR1,* and *CLU* were highly expressed at the root of the trajectory (Cluster 1). Consistently, genes from the cluster 1 were related to canonical Wnt signaling pathway, tissue regeneration, stem cell proliferation and neuronal stem cell population maintenance. Subsequently, genes from Cluster 2 were enriched with the generation of neurons, dendrite and glia cell development, such as *PTPRG, NRG3, LGI1 and SLC4A4*; and lastly, genes for neuronal function (e.g. *MAP2, SEMA5A, SYT1, SYN2, SYN3 and MYT1L*) and glial fate determination (*LAMP2, PLP1, MBP* and MOG) became dominant at the end of the trajectories fate1 and fate 2 (Cluster 3 and 4) (Figure 6H). Accordingly, the enriched GOs of genes from Cluster 4 (fate 1) were related to neurogenesis, neuron projection development, neurotransmitter secretion, and synapse organization; the enriched GOs of genes from Cluster 3 (fate 2) were associated with glial cell differentiation and myelination (Figure 6H and Table S5). Together, our data indicate that stroke-induced injury triggers activation of qNSCs, which then generate pNSCs and aNSCs, the latter of which have the potential to give rise to either neurons or oligodendrocytes(El Waly et al., 2018).

To understand relationships between regeneration and the hippocampal neurogenic lineage after stroke injury, we next explored genes involved in the activation of neurogenic lineages (qNSC1, qNSC2, pNSC, aNSC, NB). We hypothesized that genes upregulated upon injury are likely responsible for driving NSC activation. Therefore, we

compared the expression of neurogenic lineage genes between the aged and injured hippocampus (Figures 6I and 6J). Specific genes that were significantly increased in the injured hippocampus were related to regeneration, autophagy, proliferation, inflammation and metabolism (Figures 6I and 6J), some of which functions have previously been demonstrated. In mice, *Tnc*, *Gpc6*, *Cryab* and *Gbp2* were reported to promote neuron regeneration and synapse formation following stroke-induced injury (Chen et al., 2010; Chen et al., 2021; Saglam et al., 2021; Ugalde et al., 2020); *Vmp1*, *Chi3l1*, *Spp1*, *Vim* and *Itgb1* associated with autophagy, proliferation, and regeneration (Kong et al., 2018; Nishimura et al., 2021; Sojan et al., 2022; Zhao et al., 2017); and *Cyr61*, *CD63*, *Actn4*, *Ell2 and Spocd1* demonstrated to promote proliferation (Alexander et al., 2017; Chen et al., 2022; Kong et al., 2018; Liu et al., 2018; Thines et al., 2022). Furthermore, *IFI44L, RASGEF1B* and *STAT1* are linked with both inflammation and metabolic functions (Cooles et al., 2022; Leao et al., 2020) and *ACTN2, GBE1* and *NAMPT* only for metabolic functions (Ebersole et al., 2018; Gasparrini et al., 2022). Overall, the stroke-induced up-regulated molecular signatures capture a broad activation state and regeneration of the neurogenic lineage.

DISCUSSION

The existence of human adult hippocampal neurogenesis has been a topic of debate over the years. Sample rarity and technical limitations are barriers that prevent us from investigating the human postnatal hippocampus during aging and post injury. With the development of snRNA-seq technology, we are able to better understand the blueprint of hippocampal neurogenesis signatures in humans. By using snRNA-seq technology, two recent studies found no adult neurogenic trajectories in human brains (Ayhan et al., 2021; Franjic et al., 2022), while other two groups newly reported that noticeable amounts of NSCs and immature neurons were found in the adult and aged human hippocampi, supporting adult human neurogenesis capacity (Wang et al., 2022a; Zhou et al., 2022). While accumulated publications support the existence of neurogenesis in the adult human hippocampus, the homeostasis and developmental potentials of neural stem cells (NSCs) under different contexts remain unclear. Here, we have revealed the

heterogeneity and developmental trajectory of hippocampal NSCs, and captured its transcriptional molecular dynamics during postnatal development, aging and injury, which the traditional immunostainings could not uncover based on the limited sensitivity and specificity. Specially, we identified NSCs with different refined transcriptional statuses, including qNSC, pNSC and aNSC populations. Despite transcriptional similarity between qNSCs and astrocytes, we also distinguished qNSCs from astrocytes by using gene set score analysis.

The lack of specific markers has prevented the identification of neurogenic lineages in the human hippocampus for a long time. To fill this gap, we executed an integrated cross-species analysis combined with single-cell Hierarchical Poisson Factorization (scHPF) and seurat analysis to identify specific markers for human neurogenesis. In the study, we observed that both well-known and recently reported immature GC markers (Franjic et al., 2022; Hao et al., 2022; Wang et al., 2022a; Zhou et al., 2022), such as DCX, PROX1, and STMN2, are widely expressed in human GABAergic interneurons, which is consistent with Franjic's observation (Franjic et al., 2022). It suggests the risk of interneuron contamination when using these markers to identify immature GCs. We further identified new specific neuroblast markers by excluding genes expressed in human GABAergic interneurons, such as CALM3, NEUROD2, NRGN and NGN1. Thus, our findings extend our knowledge about the maker specificity of human adult hippocampal neurogenesis.

In agreement with recent studies, we also found that ETNPPL as an NSC marker (Wang et al., 2022a) was highly expressed in our identified qNSC (Figure S8A), and neuroblasts with the positivity of STMN1/2(Wang et al., 2022a) were maintained in the adult hippocampus (Figures 3B and 3C). In contrast, we did not find a comparable number of pNSCs, aNSCs and imGCs as reported in the aged group, but detected reactivated NSCs in the injured hippocampus. To explore the cause of the discrepancies, we examined the published human specimens' information from different studies which reported the existence of neuroblasts in the aged hippocampi (Zhou et al., 2022). When we integrated Zhou's snRNA-seq dataset of 14 aged donors (from 60-92 years old) with our snRNA-seq dataset, we did not detect evident pNSC, aNSC or NB populations in

their 14 aged donors (Figure S8B). To rule out the possibility of missing cell clusters caused by analysis of Zhou's data, we examined the expression of pNSC/aNSC markers (e.g., VIM, TNC) and neuroblast markers (e.g., STMN1 and NRGN), and they were not enriched in putative pNSC/aNSC/NB clusters, neither in other clusters (Figures S8C and S8D). However, $EdU^{+}PROX1^{+}$ newborn granule cells were observed in surgically resected young and adult human hippocampi from patients diagnosed with epilepsy, temporal lobe lesions or suspected low-grade glioma after *in vitro* culture (Zhou et al., 2022). One possibility is that these newborn granule cells were originated from the injury-induced activated NSCs caused by the process of hippocampus sectioning or *in vitro* culture. In addition, we noticed that two aged donors diagnosed with rectal cancer (M67Y) and uterine tumor (F52Y) in Wang's study maintained neurogenesis(Wang et al., 2022a). Given recent evidence of crosstalk between cancer and neurogenesis(Mauffrey et al., 2019; Silverman et al., 2021), we suggest that cancer might provoke neurogenesis-like status in the adult human brain. Besides, Terreros-Roncal's work showed that amyotrophic lateral sclerosis, Huntington and Parkinson's disease could increase hippocampal neurogenesis (Terreros-Roncal et al., 2021). Taking these data together, adult hippocampal neurogenesis is more easily to be detected in cases with neurological diseases, cancer and injuries(Terreros-Roncal et al., 2021; Wang et al., 2022a; Zhou et al., 2022). Therefore, the discrepancies among studies might be caused by health state differences across hippocampi, which subsequently lead to different degrees of hippocampal neurogenesis.

We constructed a developmental trajectory of NSCs in the neonatal hippocampus. Based on the trajectory and immunostaining analysis, we first deciphered transcriptional cascades of neurogenic lineages along with human hippocampal neurogenesis, and identified feature genes and transcriptional factors for each cell type. Combining the analysis of NSC properties and dynamics in neonatal, adult, aged and injured human hippocampus, our results supported the process of NSCs from active to quiescent status during aging and their re-activation under injury. In our study, we detected neuroblasts in the adult human hippocampus and active radial glial-like stem cells in the injured hippocampus both by immunostaining and snRNA-seq. The existence of neuroblasts but

not aNSCs in the adult hippocampus indicated a long maturation period of neuroblasts in humans, in agreement with previous reports that the maturation period of neuroblasts is longer in primates than in rodents (Ngwenya et al., 2015; Seki, 2020). Although a very rare number of NBs were captured by snRNA-seq, their presence was not validated by immunostaining. Because the donor died two days after the stroke, we surmise that there was not sufficient time for injury-induced aNSCs to fully differentiate into neuroblasts. However, the obviously upregulated neuronal and glial genes in the active NSC lineage in the injured hippocampus imply that these cells have the potential to generate neurons and glial cells. Taken together, our findings suggest that the reserved qNSCs in the adult human brain can be activated by stimuli such as injury or disease, and that their inherent neurogenesis capacity can be re-awakened by specific hippocampal microenvironments.

Taken together, our work deciphers the molecular heterogeneity and dynamics of human hippocampal NSCs under different contexts. This research provides valuable insights into the development, quiescence and re-activation of human hippocampal NSCs, which may explain why adult hippocampal neurogenesis is generally difficult to observe in humans but can be detected in specific cases. We realized that snRNA-seq has its limitations in distinguishing cells with very similar transcriptional signatures, and the function of the very rare number of NSCs or NBs that were captured by snRNA-seq without protein detection still needs to be further identified. Integrative analysis of epigenomic, proteomic and metabolomic features of individual hippocampal cells and non-invasive lineage tracing in human brain will be more valued in the future.

EXPERIMENTAL PROCEDURES

Resource availability

Corresponding author

For further information, please contact Tianqing Li (litq@lpbr.cn).

Materials availability

Materials and additional details can be made available from the corresponding author upon reasonable request.

Data availability

The accession numbers for the raw snRNA-seq data reported in this paper in Genome Sequence Archive (GSA): HRA003049.

Human hippocampal tissues and ethics statement

This work was approved by the ZHONG-ZHI-YI-GU Research Institute of Human Research Protection (ZZYG-YC2019-003). All donated tissues in this study were from dead patients. Tissue was collected following the guidelines recommended by the Ethical Review of Biomedical Research Involving People for tissue donation. Hippocampus tissue samples were collected after the donor patients (or family members) signed an informed consent document that was in strict observance of the legal and institutional ethics at ZHONG-ZHI-YI-GU Research Institute, Kunming University of Science and Technology. All hippocampal samples used in these studies had not been involved in any other procedures. All the protocols were in compliance with the Interim Measures for the Administration of Human Genetic Resources, administered by the Ministry of Science and Technology of China.

Human hippocampal sample collection

De-identified postnatal human hippocampus samples were obtained from the ZHONG-ZHI-YI-GU Research Institute. We recruited 10 donors from neonatal day 4 to 68 years old [neonatal (postnatal 4 days), adult (31y, 32y), aging (50y, 56y, 60y, 64y-1, 64y-2, 68y), stroke injury (48y)], consisting of 1 female and 9 males. Death reasons of these donors included: 1 congenital heart disease (postnatal day 4), 1 cerebral infarction (31y), 1 traumatic death (motor vehicle accident) (32y), 1 hypoxic-ischemic encephalopathy (stroke, 48y), 1 hypertension (50y), 3 carcinomas of the lungs (56y, 60y, 64y-2), 1 multiple organ failure (64y-1) and 1 carcinoma of the urinary bladder (68y) (Supplementary Data 1). We dissected and collected the pair of hippocampi from the donors with a short post-mortem interval (about 3-4 hours). For individuals, the left hippocampus was used for sn-RNA seq analysis; the right hippocampus was fixed for immunohistochemistry analysis. Given the differences between the rostral and caudal hippocampus (Wu and Hen, 2014), we used the anterior (AN) and mid (MI)

hippocampus containing typical DG structures for snRNA-sequencing and immunostaining.

Isolation and purification of nuclei from adult human hippocampus tissue

The cell nuclei were isolated from frozen hippocampus according to the 10x genomics nuclei isolation protocol for adult brain tissue with minor modifications (https://support.10xgenomics.com/single-cell-gene). Briefly, frozen hippocampus tissues with dentate gyrus structures were minced with surgical scissors on ice. The minced tissues were transferred into a tube with Hibernate A® (Gibco, PN-A1247501)/B27®/GlutaMAX™ (HEB) medium for equilibration. After the tissue was settled at the bottom of the tube, extra HEB was removed, leaving only enough medium to cover the tissue. Chilled lysis buffer (10 mM Tris-HCl, 10 mM NaCl, 3 mM MgCl2, and 0.1% Nonidet™ P40 Substitute (Sigma Aldrich, PN-74385) was added to the tissue and the tube was incubated on ice for 15 min with gentle shaking during the incubation. Then tissues with lysis buffer were triturated with a Pasteur pipette for 10-15 passes to obtain a single-nuclei suspension. A 30 µm MACS® SmartStrainer (Miltenyi Biotec, PN-130-098-458) was used to remove cell debris and large clumps. After centrifuging the nuclei at 500xg for 5 min at 4℃, Nuclei Wash and Resuspension Buffer (1X PBS with 1.0% BSA and 0.2U/µl RNase inhibitor (Sigma Aldrich, PN-3335399001) was added and gently pipetted for 8-10 times. After two times washing, Myelin Removal Beads II slurry (Miltenyi Biotec, PN-130-096-733) was added to the nuclei pellet. After resuspension and wash, the LS column and magnetic separation were applied to remove the myelin. The cleaned nuclei pellet was resuspended for density gradient centrifugation with a sucrose cushion. After centrifugation, 700-1,000 nuclei/µl was prepared for the following 10x Genomics Chromium capture and library construction protocol.

Single nucleus RNA library preparation for high-throughput sequencing

Single nucleus RNA-seq libraries were generated by using Chromium Single Cell 3′ Reagent Kits v3, including three main steps: 1. GEM Generation & Barcoding; 2. Post GEM-RT Cleanup & cDNA Amplification; 3. 3′ Gene Expression Library Construction.

Briefly, GEMs are generated by combining barcoded Single Cell 3′ v3 Gel Beads, a Master Mix containing cells, and Partitioning Oil onto Chromium Chip B. 5,420-18,832 nuclei were captured per channel. To achieve single nucleus resolution, nuclei were delivered at a limiting dilution. Immediately following Gel Bead-In-Emulsions (GEMs) generation, the Gel Beads were dissolved, primers containing an Illumina R1 sequence, a 16-bp 10x Barcode, a 10-bp randomer and a poly-dT primer sequence were released and mixed with cell lysate and Master Mix. After incubation of the GEMs, barcoded, full-length cDNA from poly-adenylated mRNA was generated. Barcoded, full-length cDNA was amplified via PCR to generate sufficient mass for library construction. Prior to library construction, enzymatic fragmentation and size selection were used to optimize the cDNA amplicon size. P5 primer, P7 primer, sample index sequence, and TruSeq Read 2 (read 2 primer sequence) were added via end repair, A-tailing, adaptor ligation, and PCR. The final libraries containing the P5 and P7 primers were generated by Illumina bridge amplification. Sample index sequence was incorporated as the i7 index read. TruSeq Read 1 and TruSeq Read 2 were used in paired-end sequencing (http://10xgenomics.com). Finally, the library was sequenced as 150-bp paired-end reads by using the Illumina Nova6000.

Filtering and normalization

The Cell Ranger Single-Cell Software Suit (3.0.2) (http://10xgenomics.com) (Zheng et al., 2017) was used to perform quality control and read counting of ensemble genes with default parameters (3.0.2) by mapping to the GRCh38 pre mRNA reference genome. Only confidently mapped reads with valid barcodes and unique molecular identifiers were used to generate the gene-barcode matrix. We excluded poor quality cells after the gene-cell data matrix was generated by Cell Ranger software by using the Seurat package (4.0.3) (Butler et al., 2018; Stuart et al., 2019). Only nuclei that expressed more than 200 genes and fewer than 5000-8600 (depending on the peak of enrichment genes) genes were considered. Cells with less than 200 genes or more than 8600 genes (likely cell debris and doublets) were removed. We also removed cells with more than 20% of the transcripts generated from mitochondrial genes. The co-isolation of mitochondria

during the nucleus isolation process is likely due to their association with ER. This is consistent with reports from other groups where mitochondrial DNA was detected in single-nucleus RNA-seq. In total, 33,538 genes across 92,966 single nuclei remained for subsequent analysis (Postnatal day 4 remained 17707 nuclei, 31y remained 12406 nuclei, 32y remained 11804 nuclei, 48y remained 15398 nuclei, 50y remained 5543 nuclei, 56y remained 4665 nuclei, 60y remained 7597 nuclei, 64y-1 remained 5239 nuclei, 64y-2 remained 6309 nuclei, 68y remained 6298 nuclei).

Single-cell clustering and visualization

We used the NormalizeData and FindVariableFeatures functions implemented in Seurat V3, performed standard preprocessing (log-normalization), and identified the top 2000 variable features for each individual dataset. We then identified integration anchors using the FindIntegrationAnchors function (Satija et al., 2015).We used default parameters and dimension 20 to find anchors. We then passed these anchors to the IntegrateData function to generate integrated Seurat object. To visualize the data, we used Uniform Manifold Approximation and Projection (UMAP) to project cells in 2D and 3D space based on the aligned canonical correlation analysis. Aligned canonical correlation vectors (1:20) were used to identify clusters using a shared nearest neighborhood modularity optimization algorithm.

Identification of cell types based on differentially expressed genes

Using graph-based clustering, we divided cells into 35 clusters using the FindClusters function in Seurat with resolution 1 (Butler et al., 2018). We identified 16 cell types including two unknown populations. The identified cell types are: astrocytes and qNSC (*GFAP, HES1, NOTCH2*), primed-quiescent neural stem cells (*HOPX, VIM*), active neural stem cells (*CCND2, SOX2*), neuroblast (*DCX, MYT1L*), granule cell (*SYT1, SV2B*), interneuron (*SST, CCK*), oligodendrocyte (*MOG*), microglia (*CSF1R*), pyramidal neurons (*PNN*), endothelial cells (*VWF*), oligodendrocyte precursor cell (*OLIG1, SOX10*), Reelin-expressing Cajal-Retzius cells (*RELN*), pericytes, and adult astrocyte (*S100B, ALDH1L1*). The DEGs of each cluster were identified using the FindAllMarkers

function (thresh.use = 0.25, test.use = “wilcox”) with the Seurat R package (6). We used the Wilcoxon rank-sum test (default), and genes with average expression difference > 0.5 natural log and $p < 0.05$ were selected as marker genes. Enriched GO terms of marker genes were identified using enricher function with the clusterProfiler package. Hierarchical clustering and heat-map generation were performed for single cells based on log-normalized expression values of marker genes curated from literature or identified as highly differentially expressed genes. Heat maps were generated using the Heatmap function from the Complexheatmap v2.8.0 R package. To visualize the expression of individual genes, cells were grouped into different types determined by analysis with Seurat.

Cell cycle analysis

In the cell-cycle analysis, we applied a cell-cycle related gene set with 49 genes that are higher expressed in aNSCs than in other NSCs (astrocyte-qNSC, primed NSC and neuroblast) during S and G2/M phase. UMAP plot of 92966 single-nucleus transcriptomes with points colored by putative cell-cycle phase (G0/G1, G2/M or S) using the CellCycleScoring function in Seurat (Macosko et al., 2015; Tirosh et al., 2016)

Gene set score analysis

Gene set scores (Figures 2E and 2F) were calculated by Seurat (AddModuleScore) according to previously defined RGL cell and reactive astrocyte gene sets (Clarke et al., 2018; Franjic et al., 2022; Hochgerner et al., 2018; Liddelow et al., 2017; Zamanian et al., 2012; Zhong et al., 2020) as control feature sets. Briefly, we calculated the average expression of each cell cluster on the single cell level, subtracted by the aggregated expression of control feature sets. All analyzed features are binned based on averaged expression, and the control features are randomly selected from each bin.

Pseudo-time analysis of the neurogenic lineage in neonatal and stroke-injured hippocampal cells.

The Monocle 2 R package (version 2.20.0) (Qiu et al., 2017a; Trapnell et al., 2014) were

applied to construct single cell pseudo-time trajectories (Qiu et al., 2017a; Qiu et al., 2017b; Trapnell et al., 2014) to discover developmental transitions. Cells in Seurat clusters were inferred to be the corresponding locations of the neurogenesis differentiation axis. The AS/RGLs and AS/qNSCs are at the beginning of pseudo-time in the first round of "order Cells". Dispersed genes used for pseudo-time ordering were calculated by the 'estimateDispersions' function. "DDR Tree" was applied to reduce dimensional space and the minimum spanning tree on cells was plotted by using the visualization function "plot_cell_trajectory" for Monocle 2. (Monocle function: reduceDimension(mycds, max_components = 2, method = 'DDR Tree').

Expression heatmap of highly dynamically expressed genes along the pseudotime

AS/RGLs generated two branches, granule cell subtypes GC1 and GC2, in neonatal 4 days trajectories. These branches will be characterized by distinct gene expression programs. Branched expression analysis modeling (BEAM) aims to find all genes that differ between the branches which contain 4 gene clusters in neonatal 4 days. Differentiation-related differentially expressed genes(DEGs) were obtained with a cutoff of q value $< 1 \times 10^{-4}$, and contained 4 gene clusters. In addition, the 'differentialGeneTest' function in Monocle2 R package was used to find all genes that differ between trajectory cell types (AS/qNSC, pNSC, aNSC) in stroke injury hippocampus.

Comparison of DEGs in neurogenic lineage across aging process and injury condition

We obtained significantly upregulated and down-regulated genes in aged hippocampal neurogenic lineages by comparing them with those in neonatal neurogenic lineages. Subsequently, we visualized these differentially expressed genes (DEGs) in neonatal, middle-aged and aged neurogenic lineages by violin plot and heatmap. To explore the DEGs under the stroke injury condition, we compared gene expressions of neurogenic lineages between in aged and stroke-injured hippocampus. We visualized these DEGs from neurogenic lineages in neonatal, middle-aged, aged and stroke injury hippocampus

by bubble chart to show their differential expression.

Prediction of biological functions by GO term analysis

We enriched DEGs in neurogenic lineages during aging and under stroke injury conditions by GO term analysis. Gene ontology analysis was performed by the clusterProfiler package.

Single cell hierarchical poisson factorization (scHPF) and seurat analysis (FindAllMarkers)

To identify new marker gene signatures associated with neurogenic lineages including AS/RGL, pNSC, aNSC and NB in neonatal 4 days, we factorized the data with single-cell hierarchical Poisson factorization (scHPF) (Levitin et al., 2019) and seurat analysis (FindAllMarkers) from different factors onto the neurogenic lineage. To select the optimal number of factors, first, we ran scHPF for different numbers of factors, K (from 2 to 20, interval 1). Value of K 7 optimal effect. We picked the model with K=7 and presented top 10 marker genes of scHPF analysis (Figure 3A). Meanwhile, we presented top 15 gene markers of FindAllMarkers function of seurat analysis (Figure 3B).

Immunostaining of human hippocampal tissues

The hippocampus from the right side of the brain with a short post-mortem interval was dissected and fixed with 4% paraformaldehyde (PFA) for up to 24 hours and cryoprotected in 30% sucrose at 4 °C until completely sink to the bottom. The tissue samples were frozen in OCT (Tissue-Tek) on dry ice and sectioned at 10 μm on a cryostat microtome (Leica CM1950). Tissue slides sectioned from the anterior of the hippocampus containing typical dentate gyrus structures were first incubated in blocking and permeation solution with 2% Triton X-100 (Sigma) for 2 h. Next, the sections were treated with a VECTOR TrueView autofluorescence quenching kit (Vectorlabs, PN-SP-8500-15) to reduce the innate auto-fluorescence of the human tissue, washed with 3x15min PBS (pH 7.6), and then incubated in 3% bovine serum albumin (BSA) for 1 hour at RT. Subsequently, sections were incubated overnight at 4°C with the following

primary antibodies: anti-Nestin (rabbit, 1:500, Millpore, PN-MAB5326) and anti-ki67 (mouse, 1:500, R&D system, PN-AF7649); anti-CHI3L1 (rabbit, 1:200, Novus biologicals, PN-NBPI-57913; rabbit, 1:100, Proteintech, 12036-1-AP); anti-Vimentin (rabbit, 1:300, Abcam, PN-ab137321); anti-Vimentin (mouse, 1:800, eBioscience, PN-14-9897); anti-HOPX (rabbit, 1:500, Sigma, PN-HPA030180); anti-PSA-NCAM (mouse, 1:500, millipore, PN-MAB5324). After overnight incubation, tissue sections were washed with PBS for 3x15min, and then incubated with secondary antibodies at room temperature for 2 hours: Alexa Fluor 488 AffiniPure donkey anti-rabbit IgG(H+L) (1:500, Jackson immunoresearch, PN-712-545-152), Alexa Fluor 647 AffiniPure donkey anti-rabbit IgG(H+L) (1:500, Jackson immunoresearch, PN-715-605-150). DAPI staining (Sigma, PN-32670-5mg-F) was performed and sections were washed with 1 X PBS for 3 x 15min. After washing, sections were mounted and dried, ready for microscope observation.

Terminal deoxynucleotidyl transferase dUTP nick end labeling (TUNEL) assay

Tissue sections were analyzed for DNA fragmentation using a TUNEL-based method (BOSTER, PN-MK1012). Briefly, sections were first permeabilized in 0.02% Triton X-100 overnight. To label damaged nuclei, 20 μL of the TUNEL reaction mixture (Labeling buffer, TdT, BIO-d-UTP) was added to each sample and kept at 37 °C in a humidified chamber for 120 min. Sections were a wash with PBS for 2 min and blocked with 50 μL blocking reagent at room temperature for 30 min. Then SABC buffer and DAPI were added following the protocol of BOSTER TUNELkit for the detection of apoptotic cells.

AUTHOR CONTRIBUTIONS

T.L. conceptualized, initiated and organized the project. T.L., R. Zhang and C.Z. supervised the project. T.L., R. Zhang and J.Y. designed experiments. J.Y. and R. Zhang performed experiments and helped with bioinformatics analysis. S.D. and R. Zhu analyzed the RNA-seq data. J.T., J.S., J.X. and C.H. collected hippocampus tissue. Q.Z., X.D., L.G. and J.L. performed the tissue staining and imaging. Y.Y. and N.L. prepared a single nucleus RNA library. T.L., R. Zhang. and J.Y. wrote the manuscript.

ACKNOWLEDGMENTS

This work was supported by the National Key Research and Development Program of China (2018YFA0108500 and 2020YFA0112700), the National Natural Science Foundation of China (NSFC) (32070864), the Ministry of Science and Technology of China (2022ZD0207700), Major Basic Research Project of Science and Technology of Yunnan (202001BC070001 and 202102AA100053), Key Research Project of Science and Technology of Yunnan (2018ZF007-02 and YNWR—YLXZ—2020—015).

CONFLICTS OF INTEREST

The authors declare that they have no competing interests.

REFERENCES

Alexander, L.M.M., Watters, J., Reusch, J.A., Maurin, M., Nepon-Sixt, B.S., Vrzalikova, K., Alexandrow, M.G., Murray, P.G., and Wright, K.L. (2017). Selective expression of the transcription elongation factor ELL3 in B cells prior to ELL2 drives proliferation and survival. Mol Immunol *91*, 8-16.

Alvarez-Buylla, A., and Garcia-Verdugo, J.M. (2002). Neurogenesis in adult subventricular zone. J Neurosci *22*, 629-634.

Artegiani, B., Lyubimova, A., Muraro, M., van Es, J.H., van Oudenaarden, A., and Clevers, H. (2017). A Single-Cell RNA Sequencing Study Reveals Cellular and Molecular Dynamics of the Hippocampal Neurogenic Niche. Cell Rep *21*, 3271-3284.

Ayhan, F., Kulkarni, A., Berto, S., Sivaprakasam, K., Douglas, C., Lega, B.C., and Konopka, G. (2021). Resolving cellular and molecular diversity along the hippocampal anterior-to-posterior axis in humans. Neuron *109*, 2091-2105 e2096.

Benner, E.J., Luciano, D., Jo, R., Abdi, K., Paez-Gonzalez, P., Sheng, H., Warner, D.S., Liu, C., Eroglu, C., and Kuo, C.T. (2013). Protective astrogenesis from the SVZ niche after injury is controlled by Notch modulator Thbs4. Nature *497*, 369-373.

Berg, D.A., Su, Y., Jimenez-Cyrus, D., Patel, A., Huang, N., Morizet, D., Lee, S., Shah, R., Ringeling, F.R., Jain, R.*, et al.* (2019). A Common Embryonic Origin of Stem Cells Drives Developmental and Adult Neurogenesis. Cell *177*, 654-668 e615.

Boldrini, M., Fulmore, C.A., Tartt, A.N., Simeon, L.R., Pavlova, I., Poposka, V., Rosoklija, G.B., Stankov, A., Arango, V., Dwork, A.J.*, et al.* (2018). Human Hippocampal Neurogenesis Persists throughout Aging. Cell Stem Cell *22*, 589-599 e585.

Buffo, A., Rite, I., Tripathi, P., Lepier, A., Colak, D., Horn, A.P., Mori, T., and Gotz, M. (2008). Origin and progeny of reactive gliosis: A source of multipotent cells in the injured brain. Proc Natl Acad Sci U S A *105*, 3581-3586.

Butler, A., Hoffman, P., Smibert, P., Papalexi, E., and Satija, R. (2018). Integrating single-cell transcriptomic data across different conditions, technologies, and species. Nat Biotechnol *36*, 411-420.

Chaker, Z., Aid, S., Berry, H., and Holzenberger, M. (2015). Suppression of IGF-I signals in neural stem cells enhances neurogenesis and olfactory function during aging. Aging Cell *14*, 847-856.

Chen, J., Joon Lee, H., Jakovcevski, I., Shah, R., Bhagat, N., Loers, G., Liu, H.Y., Meiners, S., Taschenberger, G., Kugler, S.*, et al.* (2010). The extracellular matrix glycoprotein tenascin-C is beneficial for spinal cord regeneration. Mol Ther *18*, 1769-1777.

Chen, Q., Wang, H., Li, Z., Li, F., Liang, L., Zou, Y., Shen, H., Li, J., Xia, Y., Cheng, Z.*, et al.* (2022). Circular RNA ACTN4 promotes intrahepatic cholangiocarcinoma progression by recruiting YBX1 to initiate FZD7 transcription. J Hepatol *76*, 135-147.

Chen, Z., Gao, M., Su, Y., Liu, P., and Sun, B. (2021). Running Promotes Transformation of Brain Astrocytes Into Neuroprotective Reactive Astrocytes and Synaptic Formation by Targeting Gpc6 Through the STAT3 Pathway. Front Physiol *12*, 633618.

Cipriani, S., Ferrer, I., Aronica, E., Kovacs, G.G., Verney, C., Nardelli, J., Khung, S., Delezoide, A.L., Milenkovic, I., Rasika, S.*, et al.* (2018). Hippocampal Radial Glial Subtypes and Their Neurogenic Potential in Human Fetuses and Healthy and Alzheimer's Disease Adults. Cereb Cortex *28*, 2458-2478.

Clarke, L.E., Liddelow, S.A., Chakraborty, C., Munch, A.E., Heiman, M., and Barres, B.A. (2018). Normal aging induces A1-like astrocyte reactivity. Proc Natl Acad Sci U S A *115*, E1896-E1905.

Cooles, F.A.H., Tarn, J., Lendrem, D.W., Naamane, N., Lin, C.M., Millar, B., Maney, N.J., Anderson, A.E., Thalayasingam, N., Diboll, J.*, et al.* (2022). Interferon-alpha-mediated therapeutic resistance in early rheumatoid arthritis implicates epigenetic reprogramming. Ann Rheum Dis.

Daynac, M., Pineda, J.R., Chicheportiche, A., Gauthier, L.R., Morizur, L., Boussin, F.D., and Mouthon, M.A. (2014). TGFbeta lengthens the G1 phase of stem cells in aged mouse brain. Stem Cells *32*, 3257-3265.

Dulken, B.W., Leeman, D.S., Boutet, S.C., Hebestreit, K., and Brunet, A. (2017). Single-Cell Transcriptomic Analysis Defines Heterogeneity and Transcriptional Dynamics in the Adult Neural Stem Cell Lineage. Cell Rep *18*, 777-790.

Ebersole, J.L., Novak, M.J., Orraca, L., Martinez-Gonzalez, J., Kirakodu, S., Chen, K.C., Stromberg, A., and Gonzalez, O.A. (2018). Hypoxia-inducible transcription factors, HIF1A and HIF2A, increase in aging mucosal tissues. Immunology *154*, 452-464.

El Waly, B., Cayre, M., and Durbec, P. (2018). Promoting Myelin Repair through In Vivo Neuroblast Reprogramming. Stem Cell Reports *10*, 1492-1504.

Encinas, J.M., Michurina, T.V., Peunova, N., Park, J.H., Tordo, J., Peterson, D.A., Fishell, G., Koulakov, A., and Enikolopov, G. (2011). Division-coupled astrocytic differentiation and age-related depletion of neural stem cells in the adult hippocampus. Cell Stem Cell *8*, 566-579.

Enwere, E., Shingo, T., Gregg, C., Fujikawa, H., Ohta, S., and Weiss, S. (2004). Aging results in reduced epidermal growth factor receptor signaling, diminished olfactory neurogenesis, and deficits in fine olfactory discrimination. J Neurosci *24*, 8354-8365.

Faiz, M., Sachewsky, N., Gascon, S., Bang, K.W., Morshead, C.M., and Nagy, A. (2015). Adult Neural Stem Cells from the Subventricular Zone Give Rise to Reactive Astrocytes in the Cortex after Stroke. Cell Stem Cell *17*, 624-634.

Franjic, D., Skarica, M., Ma, S., Arellano, J.I., Tebbenkamp, A.T.N., Choi, J., Xu, C., Li, Q., Morozov, Y.M., Andrijevic, D.*, et al.* (2022). Transcriptomic taxonomy and neurogenic trajectories of adult human, macaque, and pig hippocampal and entorhinal cells. Neuron *110*, 452-469 e414.

Garcia, A.D., Doan, N.B., Imura, T., Bush, T.G., and Sofroniew, M.V. (2004). GFAP-expressing progenitors are the principal source of constitutive neurogenesis in adult mouse forebrain. Nat Neurosci *7*, 1233-1241.

Gasparrini, M., Mazzola, F., Cuccioloni, M., Sorci, L., Audrito, V., Zamporlini, F., Fortunato, C., Amici, A., Cianci, M., Deaglio, S.*, et al.* (2022). Molecular insights into the interaction between human nicotinamide phosphoribosyltransferase and Toll-like receptor 4. J Biol Chem *298*, 101669.

Habib, N., Li, Y., Heidenreich, M., Swiech, L., Avraham-Davidi, I., Trombetta, J.J., Hession, C., Zhang, F., and Regev, A. (2016). Div-Seq: Single-nucleus RNA-Seq reveals dynamics of rare adult newborn neurons. Science *353*, 925-928.

Hao, Z.Z., Wei, J.R., Xiao, D., Liu, R., Xu, N., Tang, L., Huang, M., Shen, Y., Xing, C., Huang, W.*, et al.* (2022). Single-cell transcriptomics of adult macaque hippocampus reveals neural precursor cell populations. Nat Neurosci *25*, 805-817.

Hochgerner, H., Zeisel, A., Lonnerberg, P., and Linnarsson, S. (2018). Conserved properties of dentate gyrus neurogenesis across postnatal development revealed by single-cell RNA sequencing. Nat Neurosci *21*, 290-299.

Katsimpardi, L., Litterman, N.K., Schein, P.A., Miller, C.M., Loffredo, F.S., Wojtkiewicz, G.R., Chen, J.W., Lee, R.T., Wagers, A.J., and Rubin, L.L. (2014). Vascular and neurogenic rejuvenation of the aging mouse brain by young systemic factors. Science *344*, 630-634.

Kong, F.L., Wang, X.P., Li, Y.N., and Wang, H.X. (2018). The role of exosomes derived from cerebrospinal fluid of spinal cord injury in neuron proliferation in vitro. Artif Cells Nanomed Biotechnol *46*, 200-205.

Leao, F.B., Vaughn, L.S., Bhatt, D., Liao, W., Maloney, D., Carvalho, B.C., Oliveira, L., Ghosh, S., and Silva, A.M. (2020). Toll-like Receptor (TLR)-induced Rasgef1b expression in macrophages is regulated by NF-kappaB through its proximal promoter. Int J Biochem Cell Biol *127*, 105840.

Levitin, H.M., Yuan, J., Cheng, Y.L., Ruiz, F.J., Bush, E.C., Bruce, J.N., Canoll, P., Iavarone, A., Lasorella, A., Blei, D.M.*, et al.* (2019). De novo gene signature identification from single-cell RNA-seq with hierarchical Poisson factorization. Mol Syst Biol *15*, e8557.

Li, L., Harms, K.M., Ventura, P.B., Lagace, D.C., Eisch, A.J., and Cunningham, L.A. (2010). Focal cerebral ischemia induces a multilineage cytogenic response from adult subventricular zone that is predominantly gliogenic. Glia *58*, 1610-1619.

Liddelow, S.A., Guttenplan, K.A., Clarke, L.E., Bennett, F.C., Bohlen, C.J., Schirmer, L., Bennett, M.L., Munch, A.E., Chung, W.S., Peterson, T.C.*, et al.* (2017). Neurotoxic reactive astrocytes are induced by activated microglia. Nature *541*, 481-487.

Liu, Q., Wang, X.Y., Qin, Y.Y., Yan, X.L., Chen, H.M., Huang, Q.D., Chen, J.K., and Zheng, J.M. (2018). SPOCD1 promotes the proliferation and metastasis of glioma cells by up-regulating PTX3. Am J Cancer Res *8*, 624-635.

Llorens-Bobadilla, E., Zhao, S., Baser, A., Saiz-Castro, G., Zwadlo, K., and Martin-Villalba, A. (2015). Single-Cell Transcriptomics Reveals a Population of Dormant Neural Stem Cells that Become Activated upon Brain Injury. Cell Stem Cell *17*, 329-340.

Macosko, E.Z., Basu, A., Satija, R., Nemesh, J., Shekhar, K., Goldman, M., Tirosh, I., Bialas, A.R., Kamitaki, N., Martersteck, E.M.*, et al.* (2015). Highly Parallel Genome-wide Expression Profiling of Individual Cells Using Nanoliter Droplets. Cell *161*, 1202-1214.

Mauffrey, P., Tchitchek, N., Barroca, V., Bemelmans, A.P., Firlej, V., Allory, Y., Romeo, P.H., and Magnon, C. (2019). Progenitors from the central nervous system drive neurogenesis in cancer. Nature *569*, 672-678.

Moreno-Jimenez, E.P., Flor-Garcia, M., Terreros-Roncal, J., Rabano, A., Cafini, F., Pallas-Bazarra, N., Avila, J., and Llorens-Martin, M. (2019). Adult hippocampal neurogenesis is abundant in neurologically healthy subjects and drops sharply in patients with Alzheimer's disease. Nat Med *25*, 554-560.

Ngwenya, L.B., Heyworth, N.C., Shwe, Y., Moore, T.L., and Rosene, D.L. (2015). Age-related changes in

dentate gyrus cell numbers, neurogenesis, and associations with cognitive impairments in the rhesus monkey. Front Syst Neurosci *9*, 102.
Nishimura, N., De Battista, D., McGivern, D.R., Engle, R.E., Tice, A., Fares-Gusmao, R., Kabat, J., Pomerenke, A., Nguyen, H., Sato, S.*, et al.* (2021). Chitinase 3-like 1 is a profibrogenic factor overexpressed in the aging liver and in patients with liver cirrhosis. Proc Natl Acad Sci U S A *118*.
Obernier, K., and Alvarez-Buylla, A. (2019). Neural stem cells: origin, heterogeneity and regulation in the adult mammalian brain. Development *146*.
Ponti, G., Obernier, K., Guinto, C., Jose, L., Bonfanti, L., and Alvarez-Buylla, A. (2013). Cell cycle and lineage progression of neural progenitors in the ventricular-subventricular zones of adult mice. Proc Natl Acad Sci U S A *110*, E1045-1054.
Qiu, X., Hill, A., Packer, J., Lin, D., Ma, Y.A., and Trapnell, C. (2017a). Single-cell mRNA quantification and differential analysis with Census. Nat Methods *14*, 309-315.
Qiu, X., Mao, Q., Tang, Y., Wang, L., Chawla, R., Pliner, H.A., and Trapnell, C. (2017b). Reversed graph embedding resolves complex single-cell trajectories. Nat Methods *14*, 979-982.
Saglam, A., Calof, A.L., and Wray, S. (2021). Novel factor in olfactory ensheathing cell-astrocyte crosstalk: Anti-inflammatory protein alpha-crystallin B. Glia *69*, 1022-1036.
Satija, R., Farrell, J.A., Gennert, D., Schier, A.F., and Regev, A. (2015). Spatial reconstruction of single-cell gene expression data. Nat Biotechnol *33*, 495-502.
Seki, T. (2020). Understanding the Real State of Human Adult Hippocampal Neurogenesis From Studies of Rodents and Non-human Primates. Front Neurosci *14*, 839.
Seri, B., Garcia-Verdugo, J.M., McEwen, B.S., and Alvarez-Buylla, A. (2001). Astrocytes give rise to new neurons in the adult mammalian hippocampus. J Neurosci *21*, 7153-7160.
Silverman, D.A., Martinez, V.K., Dougherty, P.M., Myers, J.N., Calin, G.A., and Amit, M. (2021). Cancer-Associated Neurogenesis and Nerve-Cancer Cross-talk. Cancer Res *81*, 1431-1440.
Sojan, J.M., Gioacchini, G., Giorgini, E., Orlando, P., Tiano, L., Maradonna, F., and Carnevali, O. (2022). Zebrafish caudal fin as a model to investigate the role of probiotics in bone regeneration. Sci Rep *12*, 8057.
Sorrells, S.F., Paredes, M.F., Cebrian-Silla, A., Sandoval, K., Qi, D., Kelley, K.W., James, D., Mayer, S., Chang, J., Auguste, K.I.*, et al.* (2018). Human hippocampal neurogenesis drops sharply in children to undetectable levels in adults. Nature *555*, 377-381.
Steiner, B., Kronenberg, G., Jessberger, S., Brandt, M.D., Reuter, K., and Kempermann, G. (2004). Differential regulation of gliogenesis in the context of adult hippocampal neurogenesis in mice. Glia *46*, 41-52.
Stuart, T., Butler, A., Hoffman, P., Hafemeister, C., Papalexi, E., Mauck, W.M., 3rd, Hao, Y., Stoeckius, M., Smibert, P., and Satija, R. (2019). Comprehensive Integration of Single-Cell Data. Cell *177*, 1888-1902 e1821.
Terreros-Roncal, J., Moreno-Jimenez, E.P., Flor-Garcia, M., Rodriguez-Moreno, C.B., Trinchero, M.F., Cafini, F., Rabano, A., and Llorens-Martin, M. (2021). Impact of neurodegenerative diseases on human adult hippocampal neurogenesis. Science *374*, 1106-1113.
Thines, L., Gorisse, L., Li, Z., Sayedyahossein, S., and Sacks, D.B. (2022). Calmodulin activates the Hippo signaling pathway by promoting LATS1 kinase-mediated inhibitory phosphorylation of the transcriptional coactivator YAP. J Biol Chem *298*, 101839.
Tirosh, I., Izar, B., Prakadan, S.M., Wadsworth, M.H., 2nd, Treacy, D., Trombetta, J.J., Rotem, A., Rodman, C., Lian, C., Murphy, G.*, et al.* (2016). Dissecting the multicellular ecosystem of metastatic melanoma by single-cell RNA-seq. Science *352*, 189-196.

Tobin, M.K., Musaraca, K., Disouky, A., Shetti, A., Bheri, A., Honer, W.G., Kim, N., Dawe, R.J., Bennett, D.A., Arfanakis, K., *et al.* (2019). Human Hippocampal Neurogenesis Persists in Aged Adults and Alzheimer's Disease Patients. Cell Stem Cell *24*, 974-982 e973.

Trapnell, C., Cacchiarelli, D., Grimsby, J., Pokharel, P., Li, S., Morse, M., Lennon, N.J., Livak, K.J., Mikkelsen, T.S., and Rinn, J.L. (2014). The dynamics and regulators of cell fate decisions are revealed by pseudotemporal ordering of single cells. Nat Biotechnol *32*, 381-386.

Ugalde, C.L., Lewis, V., Stehmann, C., McLean, C.A., Lawson, V.A., Collins, S.J., and Hill, A.F. (2020). Markers of A1 astrocytes stratify to molecular sub-types in sporadic Creutzfeldt-Jakob disease brain. Brain Commun *2*, fcaa029.

Wang, W., Wang, M., Yang, M., Zeng, B., Qiu, W., Ma, Q., Jing, X., Zhang, Q., Wang, B., Yin, C., *et al.* (2022a). Transcriptome dynamics of hippocampal neurogenesis in macaques across the lifespan and aged humans. Cell Res *32*, 729-743.

Wang, W., Wang, M., Yang, M., Zeng, B., Qiu, W., Ma, Q., Jing, X., Zhang, Q., Wang, B., Yin, C., *et al.* (2022b). Transcriptome dynamics of hippocampal neurogenesis in macaques across the lifespan and aged humans. Cell Res.

Wu, M.V., and Hen, R. (2014). Functional dissociation of adult-born neurons along the dorsoventral axis of the dentate gyrus. Hippocampus *24*, 751-761.

Zamanian, J.L., Xu, L., Foo, L.C., Nouri, N., Zhou, L., Giffard, R.G., and Barres, B.A. (2012). Genomic analysis of reactive astrogliosis. J Neurosci *32*, 6391-6410.

Zhao, Y.G., Chen, Y., Miao, G., Zhao, H., Qu, W., Li, D., Wang, Z., Liu, N., Li, L., Chen, S., *et al.* (2017). The ER-Localized Transmembrane Protein EPG-3/VMP1 Regulates SERCA Activity to Control ER-Isolation Membrane Contacts for Autophagosome Formation. Mol Cell *67*, 974-989 e976.

Zheng, G.X., Terry, J.M., Belgrader, P., Ryvkin, P., Bent, Z.W., Wilson, R., Ziraldo, S.B., Wheeler, T.D., McDermott, G.P., Zhu, J., *et al.* (2017). Massively parallel digital transcriptional profiling of single cells. Nat Commun *8*, 14049.

Zhong, S., Ding, W., Sun, L., Lu, Y., Dong, H., Fan, X., Liu, Z., Chen, R., Zhang, S., Ma, Q., *et al.* (2020). Decoding the development of the human hippocampus. Nature *577*, 531-536.

Zhou, Y., Su, Y., Li, S., Kennedy, B.C., Zhang, D.Y., Bond, A.M., Sun, Y., Jacob, F., Lu, L., Hu, P., *et al.* (2022). Molecular landscapes of human hippocampal immature neurons across lifespan. Nature *607*, 527-533.

FIGURE LEGENDS

Figure 1. Single-nucleus transcriptomic atlas of the human hippocampus across different ages and after stroke injury

(A) Summary of the experimental strategy. The pair of hippocampi from postmortem human donors at different ages were collected. The anterior (AN) and middle (MI) parts containing dentate gyrus were used for snRNA-sequencing and immunostaining.

(B) 92,966 hippocampal single nuclei were visualized by UMAP plot and categorized into 16 major populations: adult astrocyte (Adult-AS, 1146 nuclei), astrocyte/quiescent neural stem cell (AS/qNSC, 11071 nuclei), primed NSC (pNSC, 2798 nuclei), active NSC (aNSC, 2140 nuclei), neuroblast (NB, 2607 nuclei), granule cell (GC, 24671 nuclei), interneuron (IN, 8601 nuclei), pyramidal neuron (PN, 676 nuclei), oligodendrocyte progenitor (OPC, 5396 nuclei), oligodendrocyte (OLG, 15796 nuclei),

microglia (MG, 11823 nuclei), endothelial cell (EC, 1232 nuclei), pericyte (Per, 981 nuclei), Relin-expressing Cajal–Retzius cell (CR, 218 nuclei), and two unidentified populations (UN1 and UN2, 3810 nuclei).
(C) Dot plots of representative genes specific for the indicated cell subtypes. The size of each dot represents the cell percentage of this population positive for the marker gene. The scale of the dot color represents the average expression level of the marker gene in this population.
(D) UMAP feature plots showing expression distribution of cell type specific genes in all cell populations. Astrocyte (ALDH1L1, GFAP), neural stem cell (PAX6, VIM), neuroblast (STMN2), granule cell (SV2B), oligodendrocyte progenitor (OLIG1), microglia (CSF1R), interneuron (GAD1, RELN), relin-expressing Cajal-Retzius cell (RELN), pyramidal neuron (MAP3K15) and endothelial cell (VWF) are shown. Dots, individual cells; grey, no expression; red, relative expression (log-normalized gene expression).
(E) Quantification of each cell population in the hippocampus at three different age stages and after stroke-induced injury.

Figure 2. Confirmation of neurogenic lineage and dissecting of NSC molecular heterogeneity in the postnatal human hippocampus
(A) Neurogenic lineage identification was confirmed by cross-species comparison of transcriptomic signatures. Our human data were integrated with published snRNA-seq data from mice, pigs and rhesus macaque by UMAP (Hochgerner et al., 2018, Franjic et al., 2022).
(B) Expressions of previously reported RGL, nIPC, NB and immature GC markers in the corresponding populations from our human hippocampal snRNA-seq data. RGL, radial glial cell; nIPC, neural intermediate progenitor cell; NB, neuroblast; and immature GC, immature granule cell.
(C) The AS/qNSC population was subclustered into three clusters, astrocytes, qNSC1 and qNSC2. (D) Heatmap of top 10 genes (p-value < 0.05) specific for astrocytes, qNSC1 and qNSC2 after normalization.
(E and F) Using Gene set scores (average, over genes in the set, of seurat function AddModuleScore) based on previously defined gene sets [5,7,10,23-25] to characterize RGL (E) and astrocytes (F).
(G) UMAP feature plots showing expression distribution of cell type specific genes. Astrocyte markers (S100B and GFAP), radial glial like cell markers (HOPX and LPAR1) and neuron development markers (STMN1, PROX1 and SIRT2) are shown.
(H and I) Representative GO terms of the top 1000 genes specifically expressed in pNSCs (H) and aNSCs (I).
(J) Cell-cycle phases of qNSC1, qNSC2, pNSC, aNSC and NB predicted by Cell Cycle Scoring. Each dot represents an individual cell. Steel blue, red and orange dots represent G1, S and G2/M phase cells, respectively

Figure 3. Discovery of novel markers distinguishing various types of NSCs and NBs in the human hippocampus

(A and B) Representative top genes specific for qNSC1, qNSC2, pNSC, aNSC and NB in the neonatal neurogenic lineage identified by single-cell hierarchical Poisson factorization (scHPF) (A) and FindAllMarkers function of seurat (B).
(C) UMAP visualization of several cell type specific genes of the qNSCs, pNSC and NB predicted by scHPF and FindAllMarkers.
(D) Heatmap showing that neuroblast/immature GC highly expressed genes that are previously reported by other literature were widely expressed in human hippocampal interneurons.
(E) Scatter plot showing that several NB genes predicted by scHPF and findmarker from our snRNA-seq data were also widely expressed in human hippocampal interneurons. The genes without/with low expression in the interneurons were selected as NB specific markers (red circle scope).
(F) NB specific genes selected from our snRNA-seq data were not or very low expressed in AS/qNSCs, pNSC, aNSC, NB, GC and interneurons.

Figure 4. The transcriptional dynamics predicated by RNA velocity and pseudotime reconstruction revealed developmental potentials of NSC in the neonatal human hippocampus
(A) RNA velocity analysis indicating the developmental trajectory of hippocampal neurogenic lineage at postnatal Day 4. Cell types are labeled.
(B) Representative GO terms of the differentially expressed genes compare qNSC1, qNSC2 with pNSC.
(C) Pseudotime reconstruction of the neurogenic lineages in the neonatal human hippocampus. Dots showing individual cells. Different color represents different cell types. The arrows indicate the directions of differentiation trajectories. pNSCs as the development root was successively followed by aNSCs and neuroblasts, and then separated into two branches (1 and 2), generating two types of neuronal cells N1 and N2, respectively.
(D) Expression dynamics of cell type specific genes along with the pseudotime. Each dot represents an individual cell. NSC genes (HOPX, VIM and SOX2), granule neuroblast genes (DCX and STMN2), and mature granule cell gene (SYT1) are shown.
(E) Immunostainings of radial glia (NSC) markers (HOPX and NES), active NSC markers (NES and Ki67) and neuroblast marker (PSA-NCAM). The HOPX+NES+ RGL cells and NES+Ki67+ active NSCs with long apical processes were detected in postnatal Day4 hippocampal dentate gyrus (arrows). The PSA-NCAM+ neuroblasts (green) were located across the GCL. Scale bars of HOPX/NES immunostaining are 200 μm; the magnified and further magnified cell images are 100 μm and 10 μm, respectively; the arrowhead indicates the vessel. Scale bars of KI67/NES immunostaining are 100 μm and 10 μm, respectively. Scale bars of PSA-NCAM immunostaining are 100 μm and 10 μm, respectively; arrows indicate the neuroblasts.
(F) Heatmap showing that differentially expressed genes along the pseudotime were divided into four clusters. Representative genes and enriched GO terms of each cluster are shown (p-value < 0.05).
(G) Representative NSC genes (HOPX, VIM, CHI3L1 and TNC), and neuronal genes

(NRGN, STMN2 and SV2B) were ordered by Monocle analysis along with the pseudo-time. Cell types along with the developmental trajectory were labeled by different colors.

Figure 5. Age-dependent molecular alterations of the hippocampal NSCs and NBs
(A and B) Feature plots (A) and quantification (B) of the neurogenic populations during aging. Neonatal (N), adult (Ad), aging (Ag). The neurogenic populations include qNSC1, qNSC2, pNSC, aNSC and neuroblast.
(C) The dynamic expression of some representative genes, including newly identified qNSCs genes (*LRRC3B, RHOJ,* and *SLC4A4*), NSC genes (HOPX, SOX2, VIM, NES and CHI3L1), neural progenitor or proliferation genes (ASCL1, EOMES and MKI67), and immature granule cell genes (STMN2 and DCX), in human hippocampus across neonatal (D4), adult (31y, 32y) and aging (50y, 56y, 60y, 64y-1, 64y-2, 68y).
(D) Immunostaining of classical NSC markers (HOPX, VIM and NES) in human hippocampal dentate gyrus across different ages (postnatal day 4, 32y, 50y, 56y). Scale bars, 60 μm.
(E) Violin plot showing differentially expressed genes of qNSC1 and qNSC2 in the aging group compared to the neonatal group.
(F) Representative GO terms of significantly (avg(log2FC) > 0.5, p-value < 0.05) up- and down-regulated genes in qNSC1 and qNSC2 during aging.

Figure 6. The transcriptomic signatures of the activated neurogenic lineage in the adult human injured hippocampus induced by stroke
(A) The neurogenic lineage included qNSC1, qNSC2, reactivated pNSC/aNSC and NB. Cell distribution showing by feature plots.
(B) Quantification of qNSC1, qNSC2, pNSCs, aNSCs and neuroblasts in neonatal (N), adult (Ad), aging (Ag) and stroke-injured (I) hippocampus, respectively.
(C) The dynamic expression of NSC markers (VIM, NES and CHI3L1) and oligodendrocyte progenitor cell markers (SOX10) from neonatal (N), adult (Ad), aging (Ag) and injured (I) hippocampus.
(D) Immunofluorescence images of NES (green)/Ki67 (red), VIM (red), and CHI3L1 (red)/NES (green) showing a few active NSC cells in the 48-year-old injured hippocampal dentate gyrus. The arrows indicate radial morphology NES+/KI67+, VIM+ or CHI3L1+/NES+ active NSC cells, respectively. Scale bars, 100 μm; the magnification, 20 μm.
(E and F) Integrative analysis of pNSC and aNSC from stroke injury and neonatal hippocampus showing that these cells were subclustered into 8 clusters (E), which were further annotated into pNSC, aNSC and reactive astrocytes according to gene set scores (average, over genes in the set, of seurat function AddModuleScore) (F).
(G) Pseudotime reconstruction of the neurogenic lineage in the stroke-injured human hippocampus. Different colors represent different cell types. The arrow indicates the developmental direction.
(H) Heatmap showing the expression profiles of differentially expressed genes (DEGs) in four clusters along the pseudotime. Representative DEGs and enriched GO terms of each cluster are shown.

(I) The significantly up-regulated genes in neurogenic lineage upon injury compared with aging.
(J) The GO term analysis of up-regulated genes in the neurogenic lineage upon injury compared with aging.

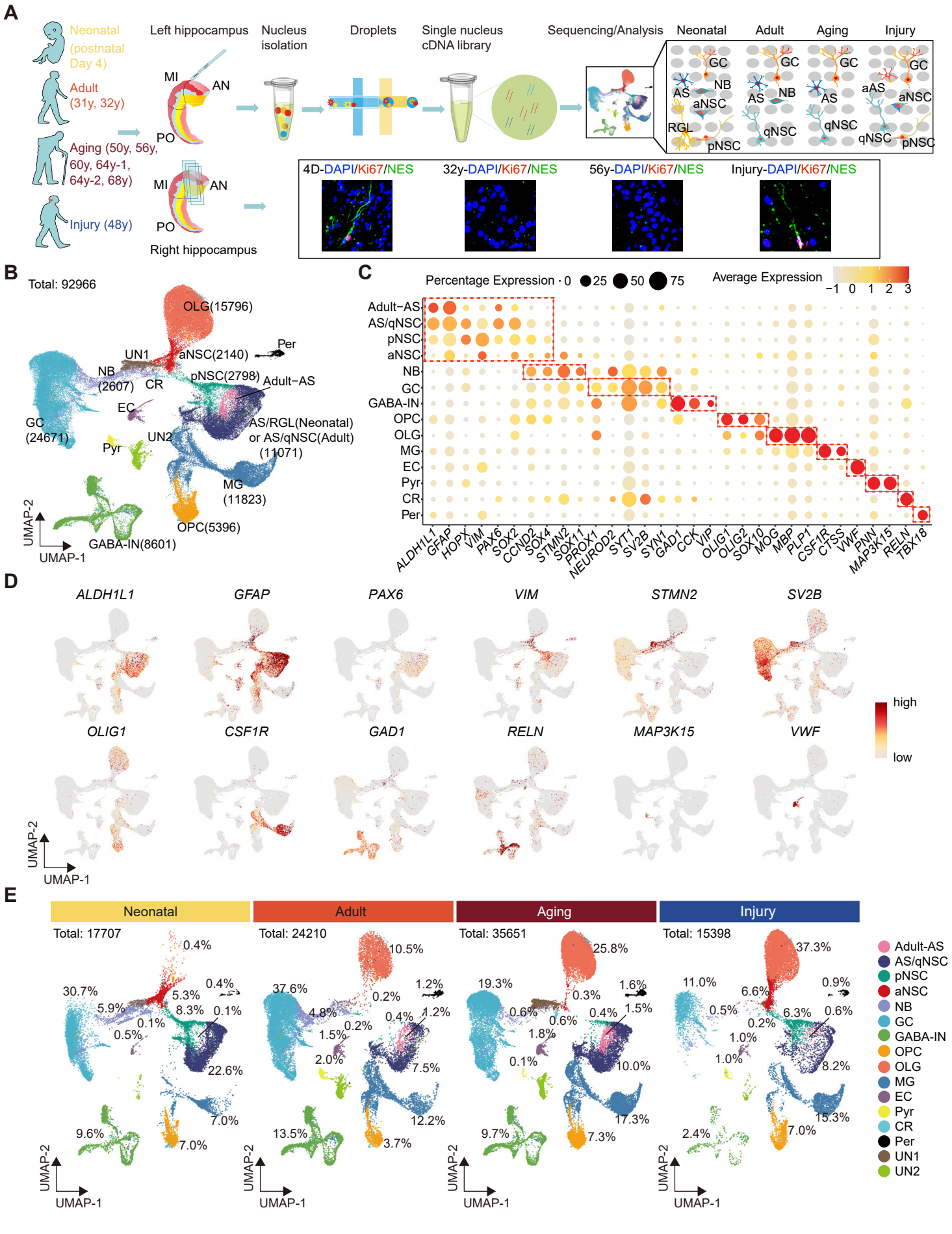
A
Neonatal (postnatal Day 4)
Adult (31y, 32y)
Aging (50y, 56y, 60y, 64y-1, 64y-2, 68y)
Injury (48y)
Left hippocampus
Right hippocampus
MI
AN
PO
Nucleus isolation
Droplets
Single nucleus cDNA library
Sequencing/Analysis
Neonatal
Adult
Aging
Injury
GC
NB
AS
aNSC
RGL
pNSC
qNSC
aAS
4D-DAPI/Ki67/NES
32y-DAPI/Ki67/NES
56y-DAPI/Ki67/NES
Injury-DAPI/Ki67/NES
B
Total: 92966
OLG(15796)
Per
UN1
aNSC(2140)
NB (2607)
CR
pNSC(2798)
Adult−AS
EC
GC (24671)
Pyr
UN2
AS/RGL(Neonatal) or AS/qNSC(Adult) (11071)
MG (11823)
OPC(5396)
GABA-IN(8601)
UMAP-2
UMAP-1
C
Percentage Expression · 0 25 50 75
Average Expression
−1 0 1 2 3
Adult−AS
AS/qNSC
pNSC
aNSC
NB
GC
GABA-IN
OPC
OLG
MG
EC
Pyr
CR
Per
ALDH1L1 GFAP HOPX VIM PAX6 SOX2 CCND2 SOX4 STMN2 SOX11 PROX1 NEUROD2 SYT1 SV2B SYN1 GAD1 CCK VIP OLIG1 OLIG2 SOX10 MOG MBP PLP1 CSF1R CTSS VWF PNN MAP3K15 RELN TBX18
D
ALDH1L1
GFAP
PAX6
VIM
STMN2
SV2B
OLIG1
CSF1R
GAD1
RELN
MAP3K15
VWF
high
low
UMAP-2
UMAP-1
E
Neonatal
Adult
Aging
Injury
Total: 17707
Total: 24210
Total: 35651
Total: 15398
Adult-AS
AS/qNSC
pNSC
aNSC
NB
GC
GABA-IN
OPC
OLG
MG
EC
Pyr
CR
Per
UN1
UN2

Figure 1

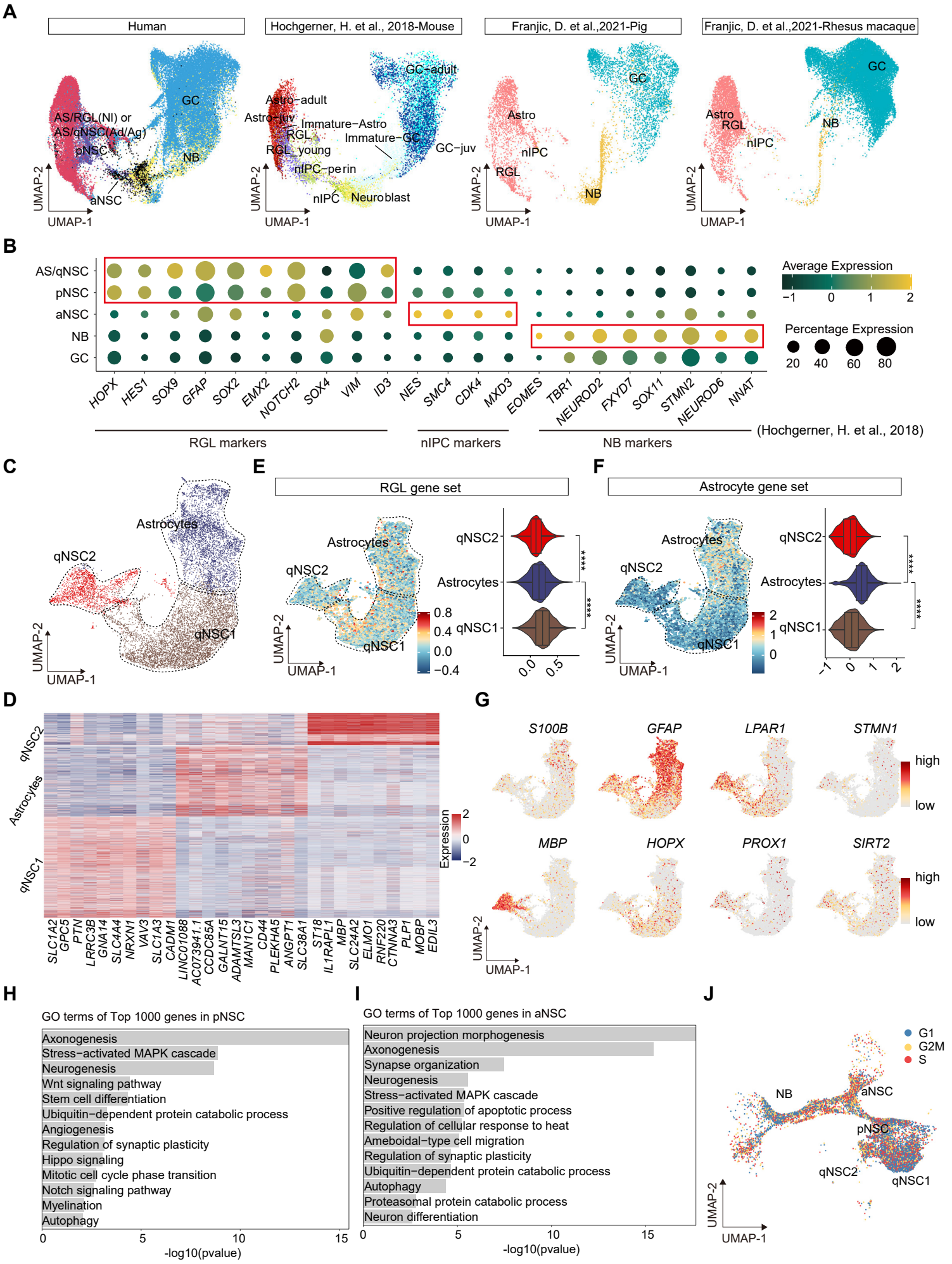
A
Human
Hochgerner, H. et al., 2018-Mouse
Franjic, D. et al.,2021-Pig
Franjic, D. et al.,2021-Rhesus macaque
AS/RGL(NI) or
AS/qNSC(Ad/Ag)
pNSC
aNSC
NB
GC
Astro-adult
Astro-juv
RGL
RGL_young
Immature-Astro
Immature-GC
GC-adult
GC-juv
nIPC-perin
nIPC
Neuroblast
Astro
nIPC
RGL
Astro
RGL
nIPC
NB
GC
UMAP-1
UMAP-2
B
AS/qNSC
pNSC
aNSC
NB
GC
HOPX
HES1
SOX9
GFAP
SOX2
EMX2
NOTCH2
SOX4
VIM
ID3
NES
SMC4
CDK4
MXD3
EOMES
TBR1
NEUROD2
FXYD7
SOX11
STMN2
NEUROD6
NNAT
RGL markers
nIPC markers
NB markers
(Hochgerner, H. et al., 2018)
Average Expression
−1
0
1
2
Percentage Expression
20
40
60
80
C
Astrocytes
qNSC2
qNSC1
UMAP-1
UMAP-2
E
RGL gene set
Astrocytes
qNSC2
qNSC1
0.8
0.4
0.0
−0.4
qNSC2
Astrocytes
qNSC1
****
****
0.0
0.5
F
Astrocyte gene set
Astrocytes
qNSC2
qNSC1
2
1
0
qNSC2
Astrocytes
qNSC1
****
****
−1
0
1
2
D
qNSC2
Astrocytes
qNSC1
Expression
2
0
−2
SLC1A2
GPC5
PTN
LRRC3B
GNA14
SLC4A4
NRXN1
VAV3
SLC1A3
CADM1
LINC01088
AC073941.1
CCDC85A
GALNT15
ADAMTSL3
MAN1C1
CD44
PLEKHA5
ANGPT1
SLC38A1
ST18
IL1RAPL1
MBP
SLC24A2
ELMO1
RNF220
CTNNA3
PLP1
MOBP
EDIL3
G
S100B
GFAP
LPAR1
STMN1
MBP
HOPX
PROX1
SIRT2
high
low
high
low
UMAP-1
UMAP-2
H
GO terms of Top 1000 genes in pNSC
Axonogenesis
Stress−activated MAPK cascade
Neurogenesis
Wnt signaling pathway
Stem cell differentiation
Ubiquitin−dependent protein catabolic process
Angiogenesis
Regulation of synaptic plasticity
Hippo signaling
Mitotic cell cycle phase transition
Notch signaling pathway
Myelination
Autophagy
0
5
10
15
-log10(pvalue)
I
GO terms of Top 1000 genes in aNSC
Neuron projection morphogenesis
Axonogenesis
Synapse organization
Neurogenesis
Stress−activated MAPK cascade
Positive regulation of apoptotic process
Regulation of cellular response to heat
Ameboidal−type cell migration
Regulation of synaptic plasticity
Ubiquitin−dependent protein catabolic process
Autophagy
Proteasomal protein catabolic process
Neuron differentiation
0
5
10
15
-log10(pvalue)
J
G1
G2M
S
NB
aNSC
pNSC
qNSC2
qNSC1
UMAP-1
UMAP-2

Figure 2

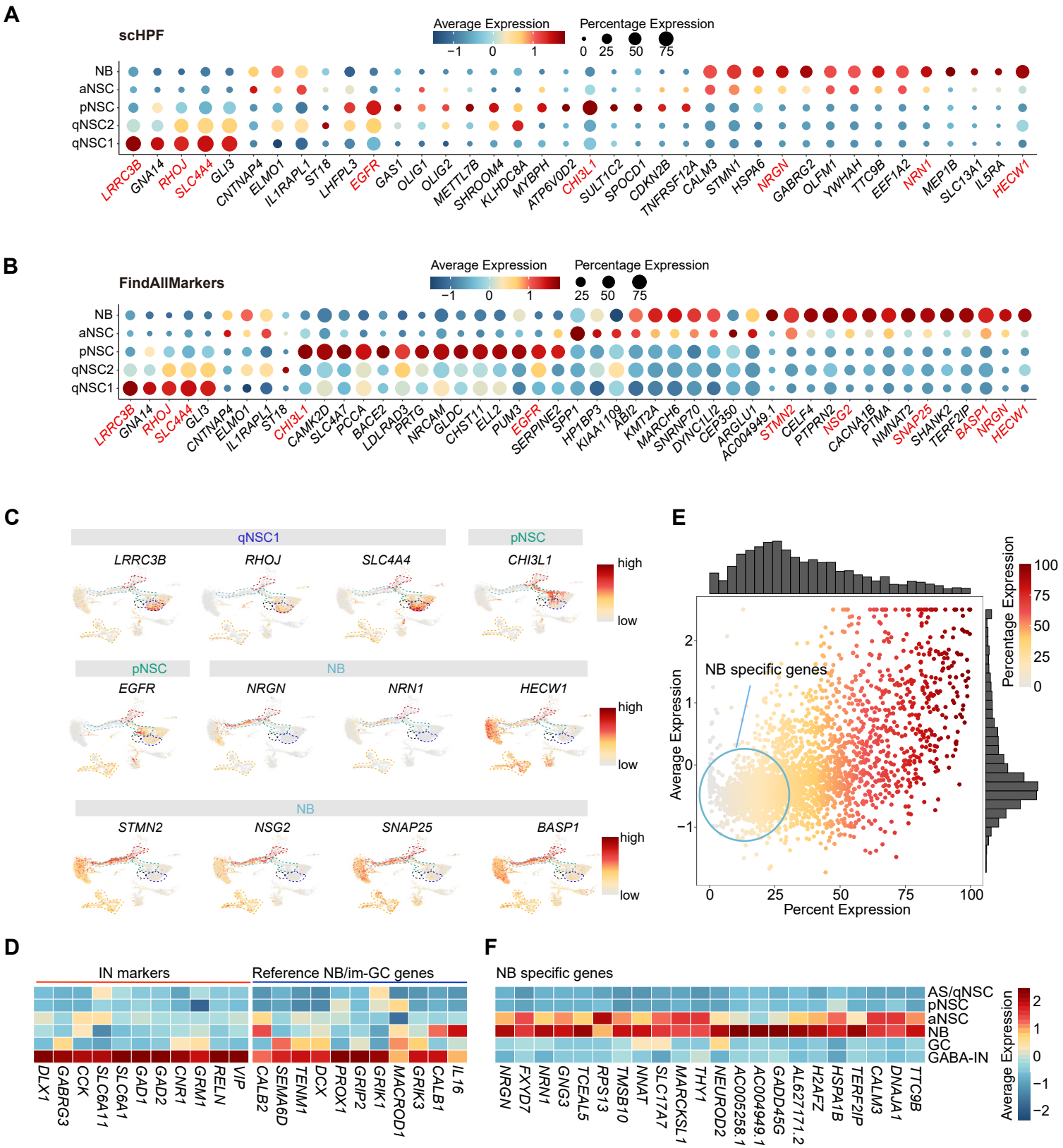
A
scHPF
Average Expression
Percentage Expression
NB
aNSC
pNSC
qNSC2
qNSC1
LRRC3B GNA14 RHOJ SLC4A4 GLI3 CNTNAP4 ELMO1 IL1RAPL1 ST18 LHFPL3 EGFR GAS1 OLIG1 OLIG2 METTL7B SHROOM4 KLHDC8A MYBPH ATP6V0D2 CHI3L1 SULT1C2 SPOCD1 CDKN2B TNFRSF12A CALM3 STMN1 HSPA6 NRGN GABRG2 OLFM1 YWHAH TTC9B EEF1A2 NRN1 MEP1B SLC13A1 IL5RA HECW1
B
FindAllMarkers
Average Expression
Percentage Expression
NB
aNSC
pNSC
qNSC2
qNSC1
LRRC3B GNA14 RHOJ SLC4A4 GLI3 CNTNAP4 ELMO1 IL1RAPL1 ST18 CHI3L1 CAMK2D SLC4A7 PCCA BACE2 LDLRAD3 PRTG NRCAM GLDC CHST11 ELL2 PUM3 EGFR SERPINE2 SPP1 HP1BP3 KIAA1109 ABI2 KMT2A MARCH6 SNRNP70 DYNC1LI2 CEP350 ARGLU1 AC004949.1 STMN2 CELF4 PTPRN2 NSG2 CACNA1B PTMA NMNAT2 SNAP25 SHANK2 TERF2IP BASP1 NRGN HECW1
C
qNSC1
pNSC
LRRC3B
RHOJ
SLC4A4
CHI3L1
high
low
pNSC
NB
EGFR
NRGN
NRN1
HECW1
high
low
NB
STMN2
NSG2
SNAP25
BASP1
high
low
E
NB specific genes
Average Expression
Percent Expression
Percentage Expression
D
IN markers
Reference NB/im-GC genes
DLX1 GABRG3 CCK SLC6A11 SLC6A1 GAD1 GAD2 CNR1 GRM1 RELN VIP
CALB2 SEMA6D TENM1 DCX PROX1 GRIP2 GRIK1 MACROD1 GRIK3 CALB1 IL16
F
NB specific genes
AS/qNSC
pNSC
aNSC
NB
GC
GABA-IN
NRGN FXYD7 NRN1 GNG3 TCEAL5 RPS13 TMSB10 NNAT SLC17A7 MARCKSL1 THY1 NEUROD2 AC005258.1 AC004949.1 GADD45G AL627171.2 H2AFZ HSPA1B TERF2IP CALM3 DNAJA1 TTC9B
Average Expression

Figure 3

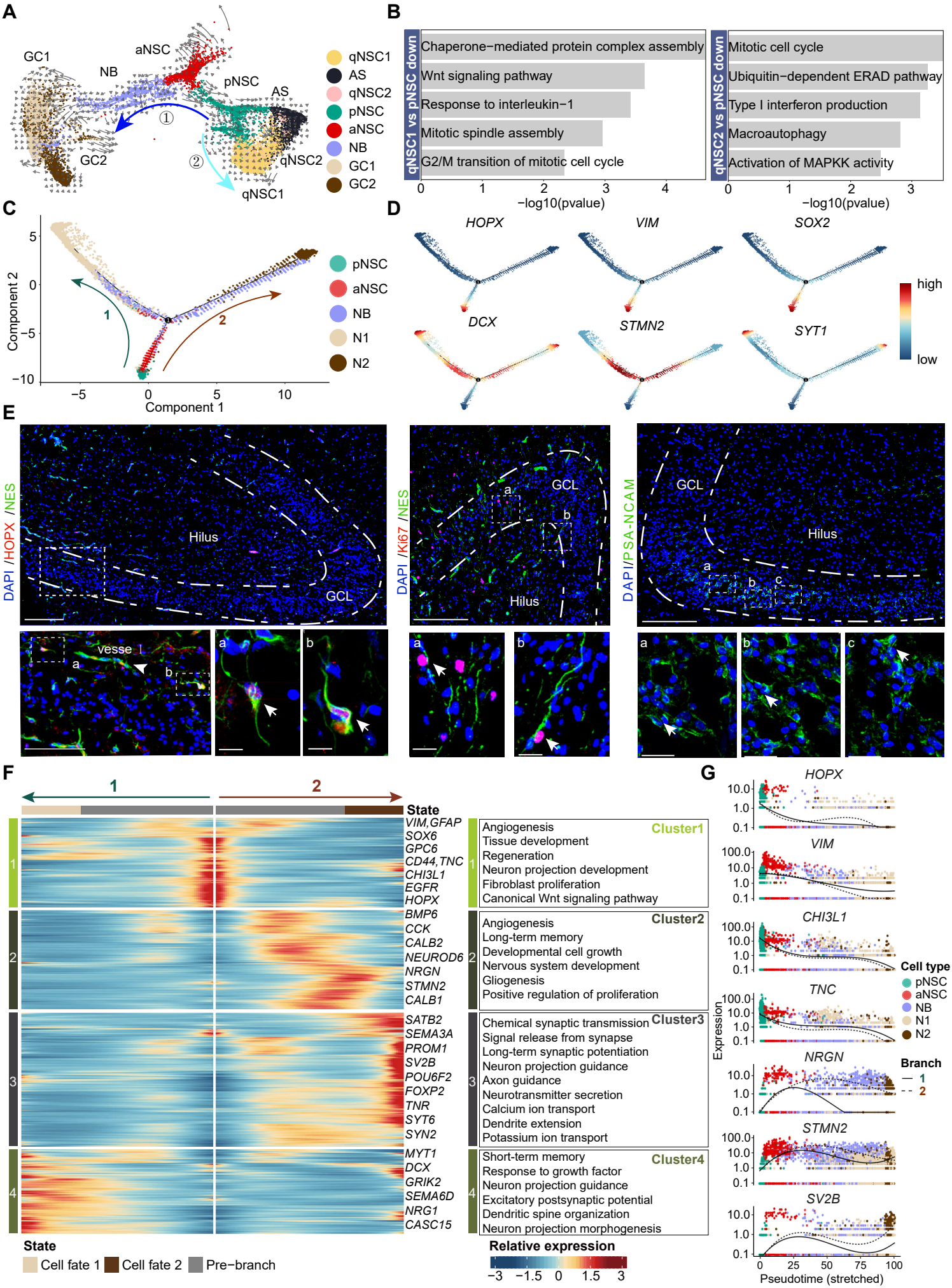
A
GC1
NB
aNSC
pNSC
AS
GC2
qNSC2
qNSC1
①
②
qNSC1
AS
qNSC2
pNSC
aNSC
NB
GC1
GC2
B
qNSC1 vs pNSC down
Chaperone−mediated protein complex assembly
Wnt signaling pathway
Response to interleukin−1
Mitotic spindle assembly
G2/M transition of mitotic cell cycle
−log10(pvalue)
qNSC2 vs pNSC down
Mitotic cell cycle
Ubiquitin−dependent ERAD pathway
Type I interferon production
Macroautophagy
Activation of MAPKK activity
−log10(pvalue)
C
Component 2
Component 1
1
2
pNSC
aNSC
NB
N1
N2
D
HOPX
VIM
SOX2
DCX
STMN2
SYT1
high
low
E
DAPI /HOPX /NES
Hilus
GCL
vesse l
DAPI /Ki67 /NES
GCL
Hilus
DAPI/PSA-NCAM
GCL
Hilus
F
1
2
State
VIM,GFAP
SOX6
GPC6
CD44,TNC
CHI3L1
EGFR
HOPX
BMP6
CCK
CALB2
NEUROD6
NRGN
STMN2
CALB1
SATB2
SEMA3A
PROM1
SV2B
POU6F2
FOXP2
TNR
SYT6
SYN2
MYT1
DCX
GRIK2
SEMA6D
NRG1
CASC15
Cluster1
Angiogenesis
Tissue development
Regeneration
Neuron projection development
Fibroblast proliferation
Canonical Wnt signaling pathway
Cluster2
Angiogenesis
Long-term memory
Developmental cell growth
Nervous system development
Gliogenesis
Positive regulation of proliferation
Cluster3
Chemical synaptic transmission
Signal release from synapse
Long-term synaptic potentiation
Neuron projection guidance
Axon guidance
Neurotransmitter secretion
Calcium ion transport
Dendrite extension
Potassium ion transport
Cluster4
Short-term memory
Response to growth factor
Neuron projection guidance
Excitatory postsynaptic potential
Dendritic spine organization
Neuron projection morphogenesis
State
Cell fate 1
Cell fate 2
Pre−branch
Relative expression
−3 −1.5 0 1.5 3
G
HOPX
VIM
CHI3L1
TNC
NRGN
STMN2
SV2B
Expression
Pseudotime (stretched)
Cell type
pNSC
aNSC
NB
N1
N2
Branch
1
2

Figure 4

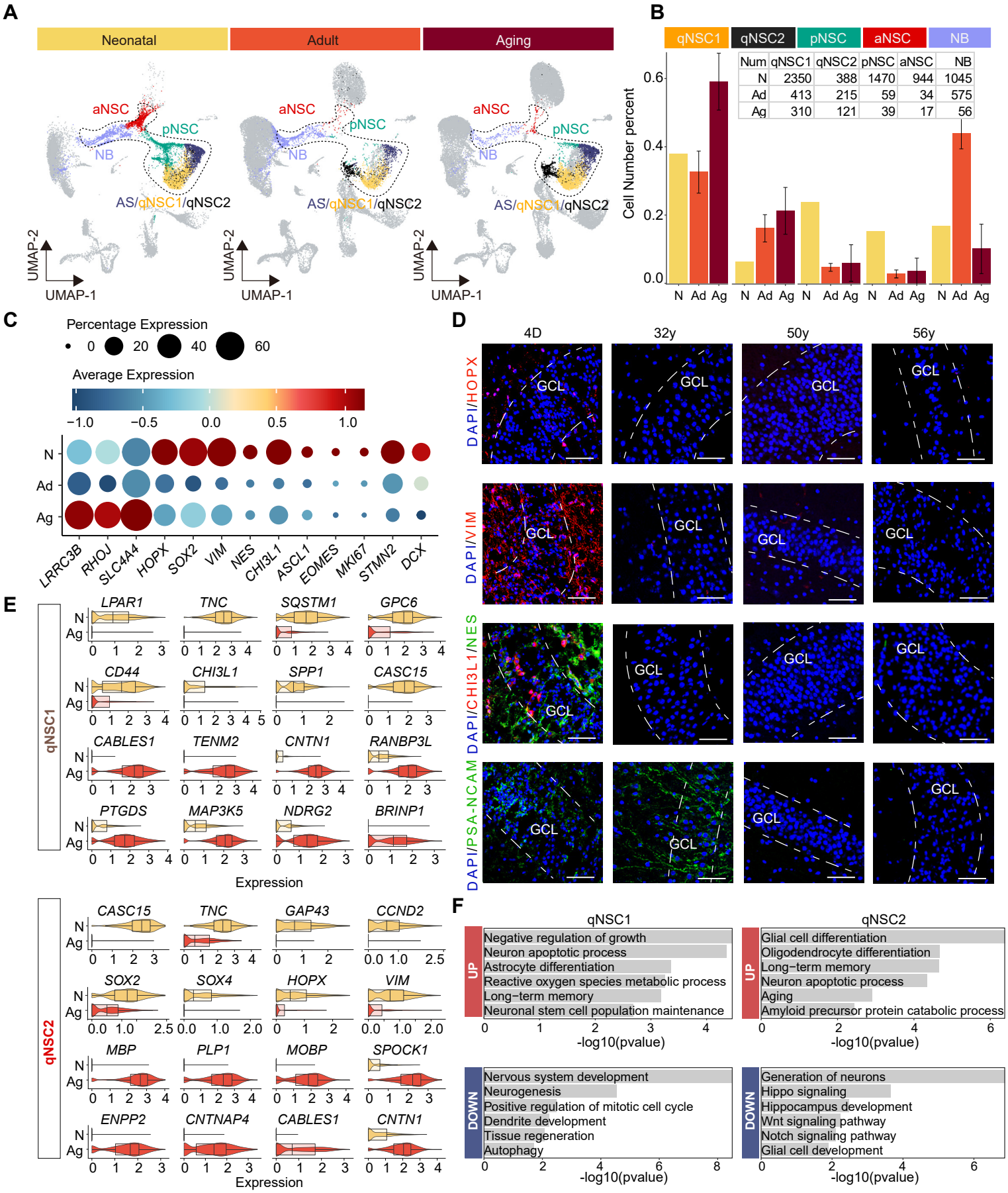

Num	qNSC1	qNSC2	pNSC	aNSC	NB
N	2350	388	1470	944	1045
Ad	413	215	59	34	575
Ag	310	121	39	17	56

Figure 5

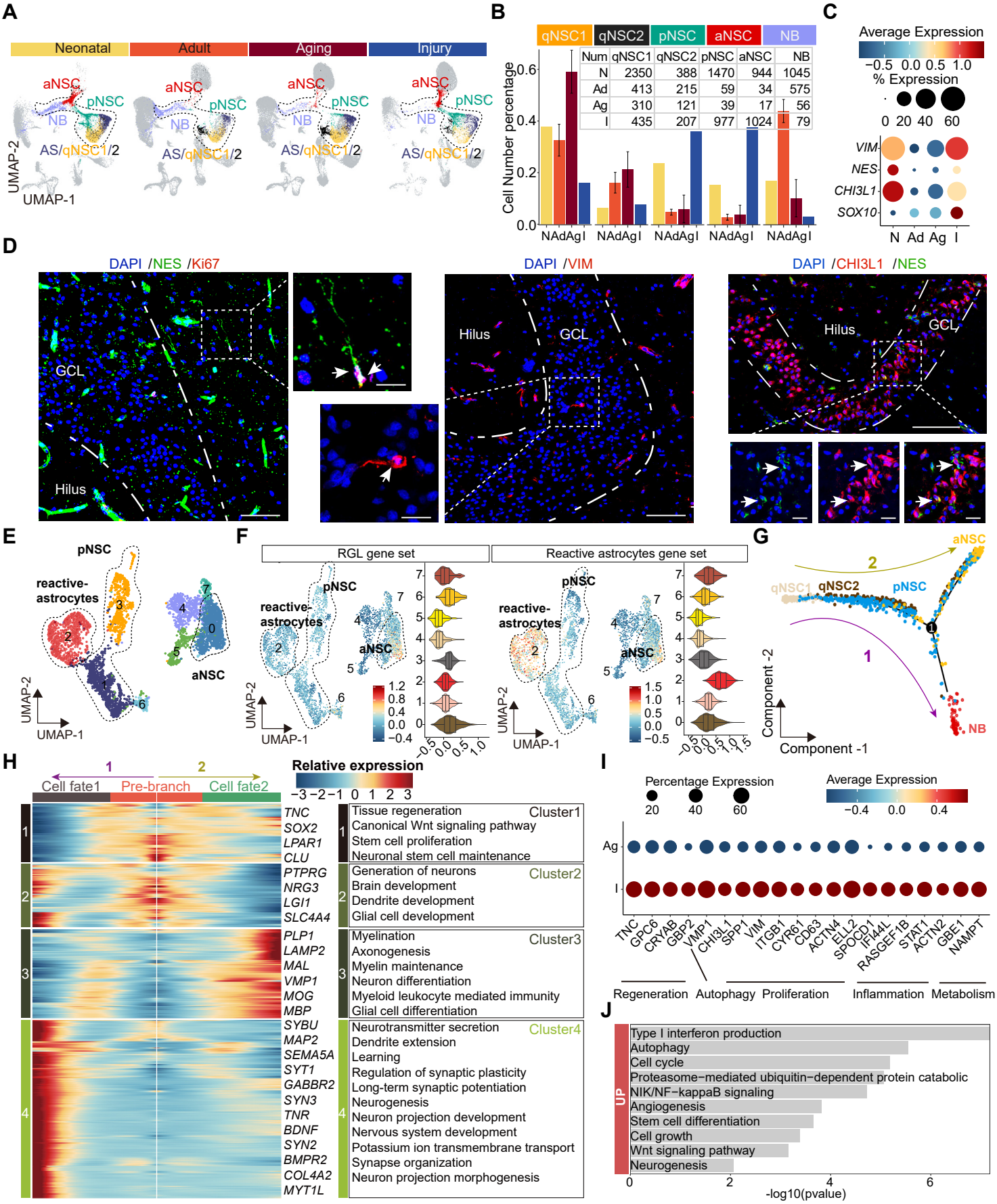
A
Neonatal
Adult
Aging
Injury
aNSC
pNSC
NB
AS/qNSC1/2
UMAP-2
UMAP-1
B
qNSC1
qNSC2
pNSC
aNSC
NB
Cell Number percentage
NAdAgI
C
Average Expression
% Expression
VIM
NES
CHI3L1
SOX10
N Ad Ag I
D
DAPI /NES /Ki67
DAPI /VIM
DAPI /CHI3L1 /NES
GCL
Hilus
E
pNSC
reactive-astrocytes
aNSC
F
RGL gene set
Reactive astrocytes gene set
G
Component -2
Component -1
H
Cell fate1
Pre-branch
Cell fate2
Relative expression
Cluster1
Tissue regeneration
Canonical Wnt signaling pathway
Stem cell proliferation
Neuronal stem cell maintenance
Cluster2
Generation of neurons
Brain development
Dendrite development
Glial cell development
Cluster3
Myelination
Axonogenesis
Myelin maintenance
Neuron differentiation
Myeloid leukocyte mediated immunity
Glial cell differentiation
Cluster4
Neurotransmitter secretion
Dendrite extension
Learning
Regulation of synaptic plasticity
Long-term synaptic potentiation
Neurogenesis
Neuron projection development
Nervous system development
Potassium ion transmembrane transport
Synapse organization
Neuron projection morphogenesis
I
Percentage Expression
Average Expression
Regeneration
Autophagy
Proliferation
Inflammation
Metabolism
J
UP
Type I interferon production
Autophagy
Cell cycle
Proteasome−mediated ubiquitin−dependent protein catabolic
NIK/NF−kappaB signaling
Angiogenesis
Stem cell differentiation
Cell growth
Wnt signaling pathway
Neurogenesis
-log10(pvalue)

Figure 6

Supplemental Information

Deciphering molecular heterogeneity and dynamics of neural stem cells in human hippocampal development, aging, and injury

Junjun Yao, Shaoxing Dai, Ran Zhu, Ju Tan, Qiancheng Zhao, Yu Yin, Jiansen Sun, Xuewei Du, Longjiao Ge, Jianhua Xu, Chunli Hou, Nan Li, Jun Li, Weizhi Ji, Chuhong Zhu, Runrui Zhang, Tianqing Li

Supplementary figure legends

Figure S1. Cell atlas of human hippocampus across different ages and post stoke-induced injury. (A) Visualization of major cell types from human hippocampal snRNA-seq data by using 3D UMAP. (B) Cell atlas of each human hippocampal sample. Different colors indicate different samples. (C) Heatmap of top 50 genes (p-value < 0.05) specific for each major population after normalization. Adult-AS, adult astrocyte; AS/qNSC, astrocyte/quiescent neural stem cell; pNSC, primed NSC; aNSC, active neural stem cell; NB, neuroblast; GC, granule cell; GABA-IN, GABAgeric-interneuron; Pyr, pyramidal neuron; OPC, oligodendrocyte progenitor cell; OLG, oligodendrocyte; MG, microglia; EC, endothelia cell; Per, pericyte; CR, Relin-expressing Cajal-Retzius cell; Unknown1 (UN1); Unknown2 (UN2). Related to Figure 1.

Figure S2. Reported neuroblast genes were widely distributed in the adult human interneurons. (A) Transcriptional congruence of granule cell lineage and interneuron population between our dataset and published mouse, macaque and human transcriptome datasets. The matrix plot indicates the similarity scores of given human hippocampal cell populations from our dataset (rows) assigned to the corresponding literature-annotated cell types (columns). (B) Neuroblast genes reported by several literatures were widely distributed in the adult human interneurons from 10 individuals. (C) Our identified neuroblast specific genes were absent in the adult human interneurons. Related to Figure 3.

Figure S3. Pseudotime reconstruction of the neurogenic lineage development in the neonatal Day 4 human hippocampus. (A) Cells during neurogenic lineage development were ordered by Monocle analysis along pseudo-time. (B) Cell types located at developmental trajectory were labeled by different colors. (C and D) Heatmap (C) and UMAP (D) visualization of distinct differentially expressed genes between N1 and N2. (E) The dynamic changes of representative genes along the pseudo-time were shown by Monocle analysis. Cell types along with the developmental trajectory were labeled by different colors. (F) Heatmap showing expression dynamics of transcriptional factors (TFs) along the neurogenesis trajectory. The representative TFs in each cluster were shown on the right. Related to Figure 4.

Figure S4. Alterations of the neurogenic lineage in human hippocampus during aging. (A) Bubble plots showing our identified pNSCs, aNSCs and NBs from 10 individuals still express neural stem cell and neuroblast marker genes during aging despite their rare number. 48y donor was a stroke sample. (B) Immunostainings of classical NSC markers (HOPX, VIM and NES), pNSC gene CHI3L1 identified by us and neuroblast marker PSA-NCAM in human hippocampal dentate gyrus across different ages (postnatal day 4, 32y and 56y). Scale bars: 4D-500 μm, 32y-800 μm, 56y-600 μm. Related to Figure 5.

Figure S5. Differentially expressed genes and enrichment functions in pNSC, aNSC, and NB along aging, respectively. (A) Heatmap showing differentially expressed genes (DEGs) between aging pNSC and neonatal pNSC (p-value < 0.05). (B and C) Representative GO terms of significantly up-regulated (B) and down-regulated (C) genes during pNSC aging (avg(log2FC) > 0.5, p-value < 0.05). (D) Heatmap showing DEGs between aging aNSC and neonatal aNSC (p-value < 0.05). (E and F) Representative GO terms of significantly up- regulated (E) and down-regulated (F) genes during aNSC aging (avg(log2FC) > 0.5, p-value < 0.05). (G) Heatmap showing DEGs between aging NB and neonatal NB (p-value < 0.05). (H and I) Representative GO terms of significantly up- regulated (H) and down-regulated (I) genes during NB aging (avg(log2FC) > 0.5, p-value < 0.05). Related to Figure 5.

Figure S6. Stroke injury induced hippocampal cell apoptosis, astrocyte reactivation and neuronal damages. (A) Representative GO terms of upregulated genes in stroke-injured hippocampal GCs and INs, compared with the normal aged hippocampus. (B) Genes relative to apoptosis, DNA damage and autophagy were significantly upregulated in the stroke-injured hippocampus, compared with the normal aged hippocampus. I, injury; Ag, aging. (C) TUNEL assay showing obvious cell apoptosis in the 48y dentate gyrus, but not in other adult samples, which confirmed the stroke caused hippocampal injury. Scale bars, 500 μm. (D) CHI3L1 and VIM co-immunostaining showing some CHI3L1+VIM+ and CHI3L1+VIM- cells exhibited morphologies of reactive astrocyte (arrowhead) and neuron (arrow) in the GCL and hilus, respectively. Scale bars, 500 μm; the magnified images, 100 μm and 20 μm. Related to Figure 6.

Figure S7. Initially defined pNSCs and aNSCs from stroke-injured hippocampus contained reactive astrocytes and reactivated NSCs. The integrative analysis of single cell data was based on initially defined pNSC and aNSC populations from the neonatal Day 4 and 48y-stroke injury hippocampus. (A) Heatmap of top 10 genes (p-value < 0.05) specific for each major cluster after normalization, relative to Fig. 6E. (B) The fraction of subpopulations in total cells (cluster 0-7). (C) UMAP feature plots showing expression distribution of cell type specific genes in cell subpopulations, including RGL marker genes (VIM, HOPX, LPAR1 and SOX2), neurogenic development genes (STMN1), and reactive astrocytes marker gene (OSMR, TIMP and LGALS3). (D) The dynamic expression of cell type specific genes along the pseudotime. Each dot represents an individual cell. These representative genes included RGL genes PAX6 and HOPX, reactivated NSC genes VIM, CD44, TNC, CHI3L1 and SOX2, and cell cycle genes CKAP5 and RANGAP1, and neuroblast gene STMN2. Related to Figure 6.

Figure S8. Integration of our snRNA-seq dataset with other published data. (A) ETNPPL as a new NSC marker and STMN1/STMN2 as new immature neuron markers validated in Wang's study were verified in our study. (B) Integration of Zhou's snRNA-seq dataset of 14 aged donors (from 60-92 years old) with our snRNA-seq dataset. We did not detect evident pNSC, aNSC or NB populations in their dataset (circle with a dotted line). (C and D) UMAP visualization of pNSC/aNSC markers (TNC and VIM) (C), and neuroblast markers (STMN1 and NRGN) (D) in our and Zhou's snRNA-seq dataset. Related to discussion.

Supplementary tables

Supplementary table 1. Patient information and the expression of findmarker genes used to identify cell populations in UMAP. Related to Figure 1
Supplementary table 2. Potential marker genes identified by Findallmarker and scHPF. Related to Figure 3.
Supplementary table 3. Genes and enriched GO terms of 4 clusters from neonatal neurogenic lineage trajectory. Related to Figure 4.
Supplementary table 4. Genes and enriched GO terms of qNSC1 and qNSC2 during aging. Related to Figure 5.
Supplementary table 5. Genes and enriched GO terms of 4 clusters from injury neurogenic lineage trajectory. Related to Figure 6.

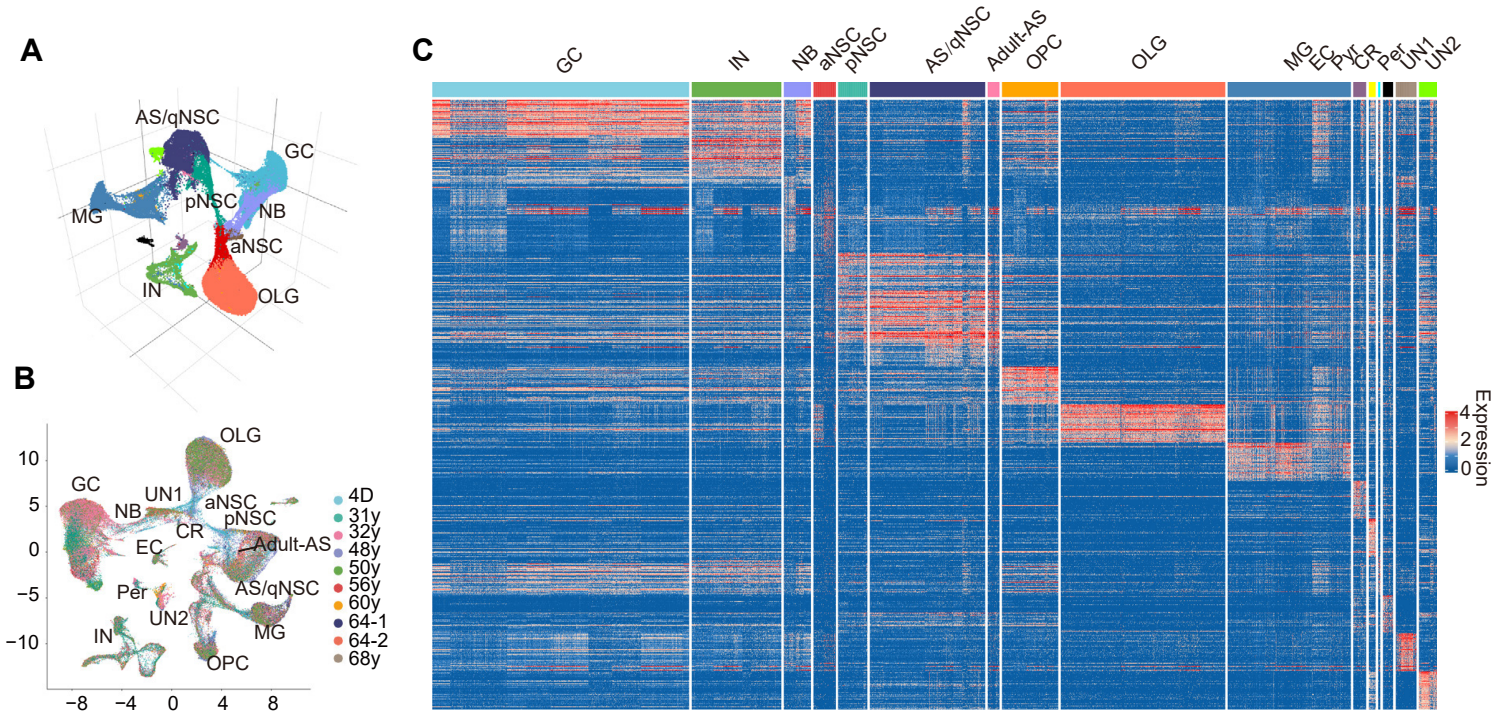
A
AS/qNSC
GC
MG
pNSC
NB
aNSC
IN
OLG
B
OLG
GC
UN1
NB
aNSC
pNSC
CR
EC
Adult-AS
Per
AS/qNSC
UN2
IN
MG
OPC
10
5
0
−5
−10
−8
−4
0
4
8
4D
31y
32y
48y
50y
56y
60y
64-1
64-2
68y
C
GC
IN
NB
aNSC
pNSC
AS/qNSC
Adult-AS
OPC
OLG
MG
EC
Pyr
CR
Per
UN1
UN2
Expression
4
2
0

Figure S1

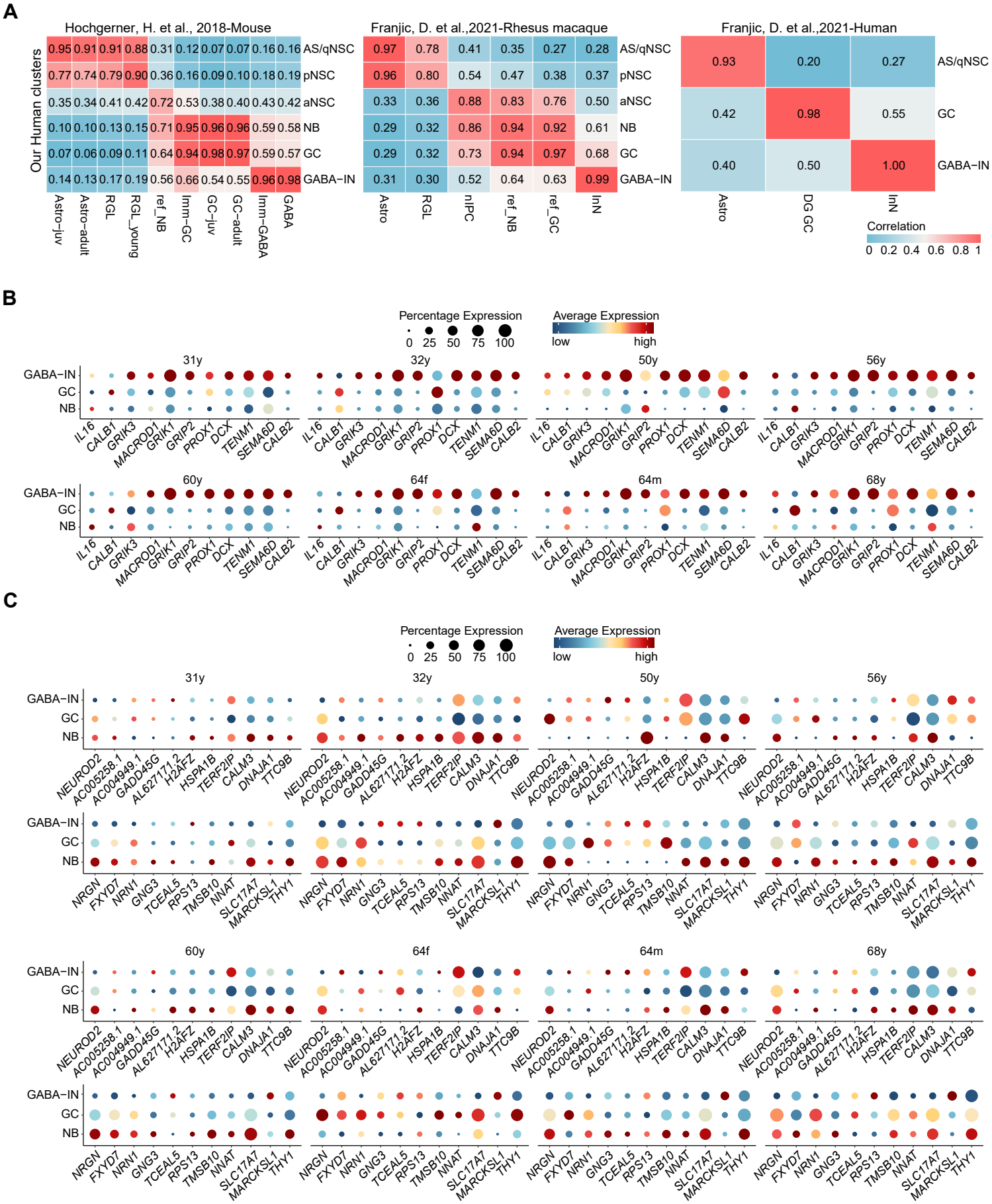
A
Hochgerner, H. et al., 2018-Mouse
Our Human clusters
AS/qNSC
pNSC
aNSC
NB
GC
GABA−IN
Astro−juv
Astro−adult
RGL
RGL_young
ref_NB
Imm−GC
GC−juv
GC−adult
Imm−GABA
GABA
Franjic, D. et al.,2021-Rhesus macaque
Astro
RGL
nIPC
ref_NB
ref_GC
InN
Franjic, D. et al.,2021-Human
DG GC
Correlation
0 0.2 0.4 0.6 0.8 1
B
Percentage Expression
0 25 50 75 100
Average Expression
low
high
31y
32y
50y
56y
60y
64f
64m
68y
IL16
CALB1
GRIK3
MACROD1
GRIK1
GRIP2
PROX1
DCX
TENM1
SEMA6D
CALB2
C
NEUROD2
AC005258.1
AC004949.1
GADD45G
AL627171.2
H2AFZ
HSPA1B
TERF2IP
CALM3
DNAJA1
TTC9B
NRGN
FXYD7
NRN1
GNG3
TCEAL5
RPS13
TMSB10
NNAT
SLC17A7
MARCKSL1
THY1

Figure S2

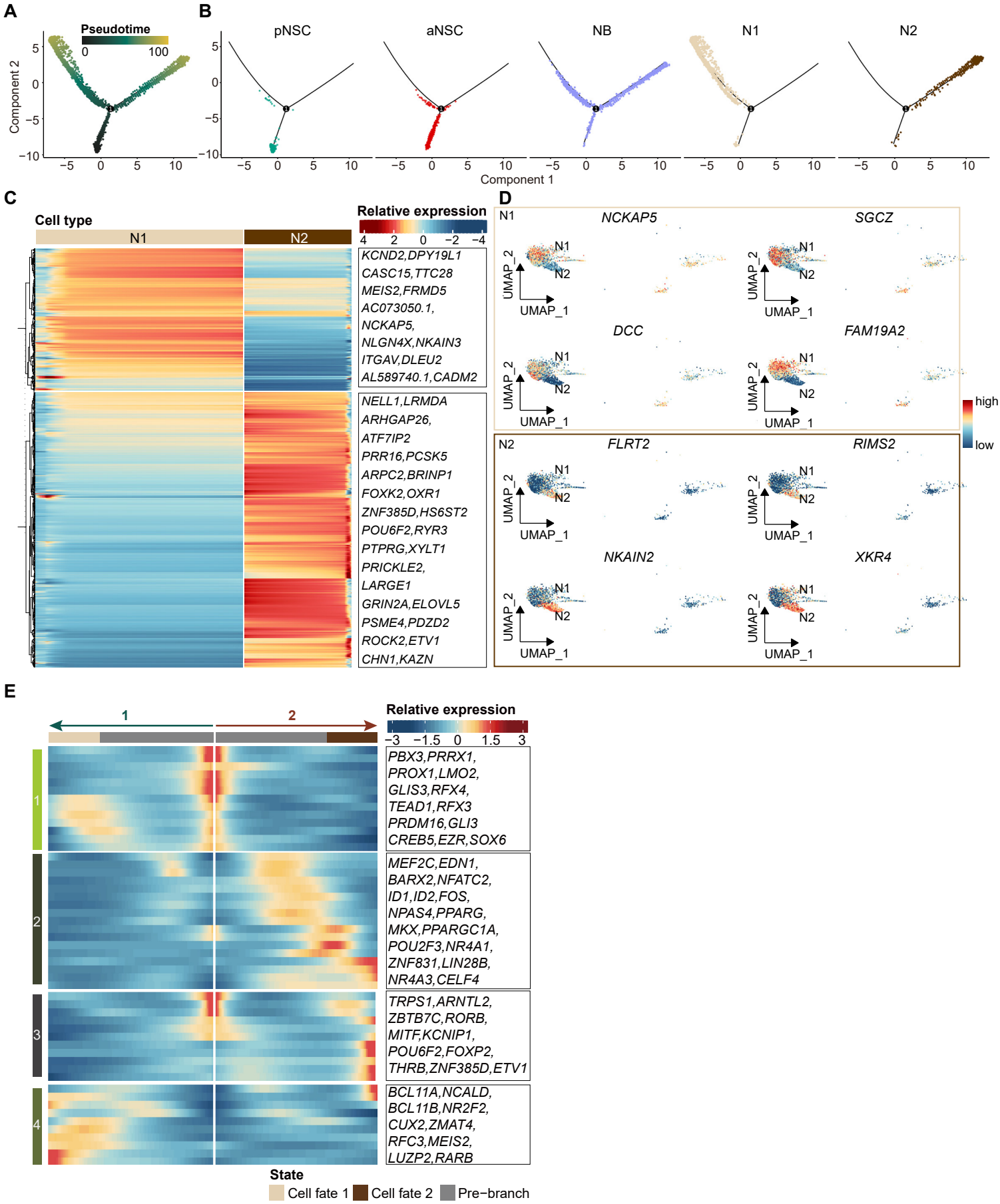
A
Pseudotime
0
100
Component 2
B
pNSC
aNSC
NB
N1
N2
Component 1
C
Cell type
N1
N2
Relative expression
4 2 0 −2 −4
KCND2,DPY19L1
CASC15,TTC28
MEIS2,FRMD5
AC073050.1,
NCKAP5,
NLGN4X,NKAIN3
ITGAV,DLEU2
AL589740.1,CADM2
NELL1,LRMDA
ARHGAP26,
ATF7IP2
PRR16,PCSK5
ARPC2,BRINP1
FOXK2,OXR1
ZNF385D,HS6ST2
POU6F2,RYR3
PTPRG,XYLT1
PRICKLE2,
LARGE1
GRIN2A,ELOVL5
PSME4,PDZD2
ROCK2,ETV1
CHN1,KAZN
D
N1
NCKAP5
SGCZ
DCC
FAM19A2
N2
FLRT2
RIMS2
NKAIN2
XKR4
UMAP_1
UMAP_2
high
low
E
1
2
Relative expression
−3 −1.5 0 1.5 3
PBX3,PRRX1,
PROX1,LMO2,
GLIS3,RFX4,
TEAD1,RFX3
PRDM16,GLI3
CREB5,EZR,SOX6
MEF2C,EDN1,
BARX2,NFATC2,
ID1,ID2,FOS,
NPAS4,PPARG,
MKX,PPARGC1A,
POU2F3,NR4A1,
ZNF831,LIN28B,
NR4A3,CELF4
TRPS1,ARNTL2,
ZBTB7C,RORB,
MITF,KCNIP1,
POU6F2,FOXP2,
THRB,ZNF385D,ETV1
BCL11A,NCALD,
BCL11B,NR2F2,
CUX2,ZMAT4,
RFC3,MEIS2,
LUZP2,RARB
State
Cell fate 1
Cell fate 2
Pre−branch

Figure S3

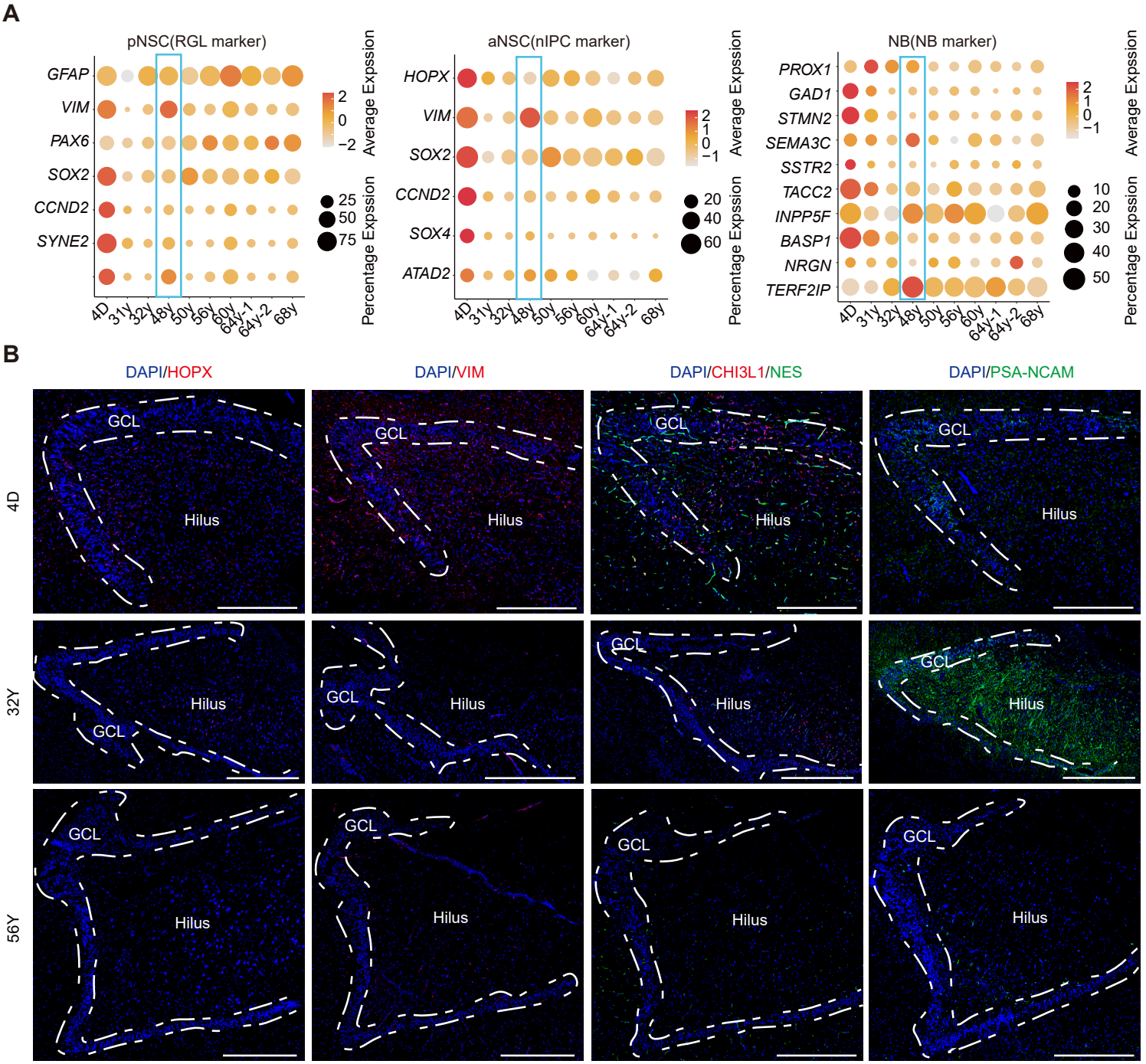
A
pNSC(RGL marker)
GFAP
VIM
PAX6
SOX2
CCND2
SYNE2
aNSC(nIPC marker)
HOPX
VIM
SOX2
CCND2
SOX4
ATAD2
NB(NB marker)
PROX1
GAD1
STMN2
SEMA3C
SSTR2
TACC2
INPP5F
BASP1
NRGN
TERF2IP
4D
31Y
32Y
48Y
50Y
56Y
60Y
64Y-1
64Y-2
68Y
Average Expssion
Percentage Expssion
B
DAPI/HOPX
DAPI/VIM
DAPI/CHI3L1/NES
DAPI/PSA-NCAM
4D
32Y
56Y
GCL
Hilus

Figure S4

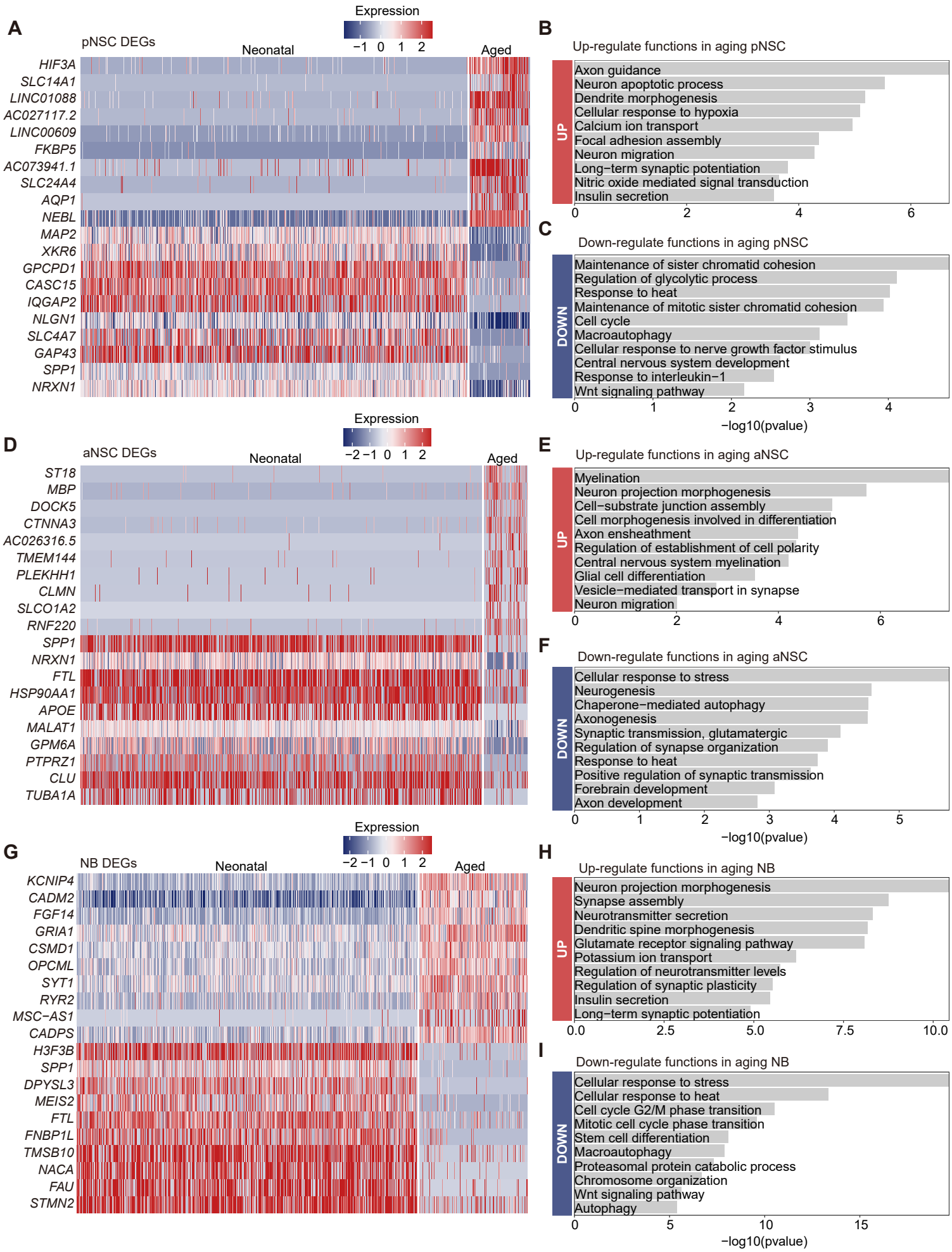
A
pNSC DEGs
Expression
−1 0 1 2
Neonatal
Aged
HIF3A
SLC14A1
LINC01088
AC027117.2
LINC00609
FKBP5
AC073941.1
SLC24A4
AQP1
NEBL
MAP2
XKR6
GPCPD1
CASC15
IQGAP2
NLGN1
SLC4A7
GAP43
SPP1
NRXN1
B
Up-regulate functions in aging pNSC
UP
Axon guidance
Neuron apoptotic process
Dendrite morphogenesis
Cellular response to hypoxia
Calcium ion transport
Focal adhesion assembly
Neuron migration
Long−term synaptic potentiation
Nitric oxide mediated signal transduction
Insulin secretion
0 2 4 6
C
Down-regulate functions in aging pNSC
DOWN
Maintenance of sister chromatid cohesion
Regulation of glycolytic process
Response to heat
Maintenance of mitotic sister chromatid cohesion
Cell cycle
Macroautophagy
Cellular response to nerve growth factor stimulus
Central nervous system development
Response to interleukin−1
Wnt signaling pathway
0 1 2 3 4
−log10(pvalue)
D
aNSC DEGs
Expression
−2 −1 0 1 2
Neonatal
Aged
ST18
MBP
DOCK5
CTNNA3
AC026316.5
TMEM144
PLEKHH1
CLMN
SLCO1A2
RNF220
SPP1
NRXN1
FTL
HSP90AA1
APOE
MALAT1
GPM6A
PTPRZ1
CLU
TUBA1A
E
Up-regulate functions in aging aNSC
UP
Myelination
Neuron projection morphogenesis
Cell−substrate junction assembly
Cell morphogenesis involved in differentiation
Axon ensheathment
Regulation of establishment of cell polarity
Central nervous system myelination
Glial cell differentiation
Vesicle−mediated transport in synapse
Neuron migration
0 2 4 6
F
Down-regulate functions in aging aNSC
DOWN
Cellular response to stress
Neurogenesis
Chaperone−mediated autophagy
Axonogenesis
Synaptic transmission, glutamatergic
Regulation of synapse organization
Response to heat
Positive regulation of synaptic transmission
Forebrain development
Axon development
0 1 2 3 4 5
−log10(pvalue)
G
NB DEGs
Expression
−2 −1 0 1 2
Neonatal
Aged
KCNIP4
CADM2
FGF14
GRIA1
CSMD1
OPCML
SYT1
RYR2
MSC−AS1
CADPS
H3F3B
SPP1
DPYSL3
MEIS2
FTL
FNBP1L
TMSB10
NACA
FAU
STMN2
H
Up-regulate functions in aging NB
UP
Neuron projection morphogenesis
Synapse assembly
Neurotransmitter secretion
Dendritic spine morphogenesis
Glutamate receptor signaling pathway
Potassium ion transport
Regulation of neurotransmitter levels
Regulation of synaptic plasticity
Insulin secretion
Long−term synaptic potentiation
0.0 2.5 5.0 7.5 10.0
I
Down-regulate functions in aging NB
DOWN
Cellular response to stress
Cellular response to heat
Cell cycle G2/M phase transition
Mitotic cell cycle phase transition
Stem cell differentiation
Macroautophagy
Proteasomal protein catabolic process
Chromosome organization
Wnt signaling pathway
Autophagy
0 5 10 15
−log10(pvalue)

Figure S5

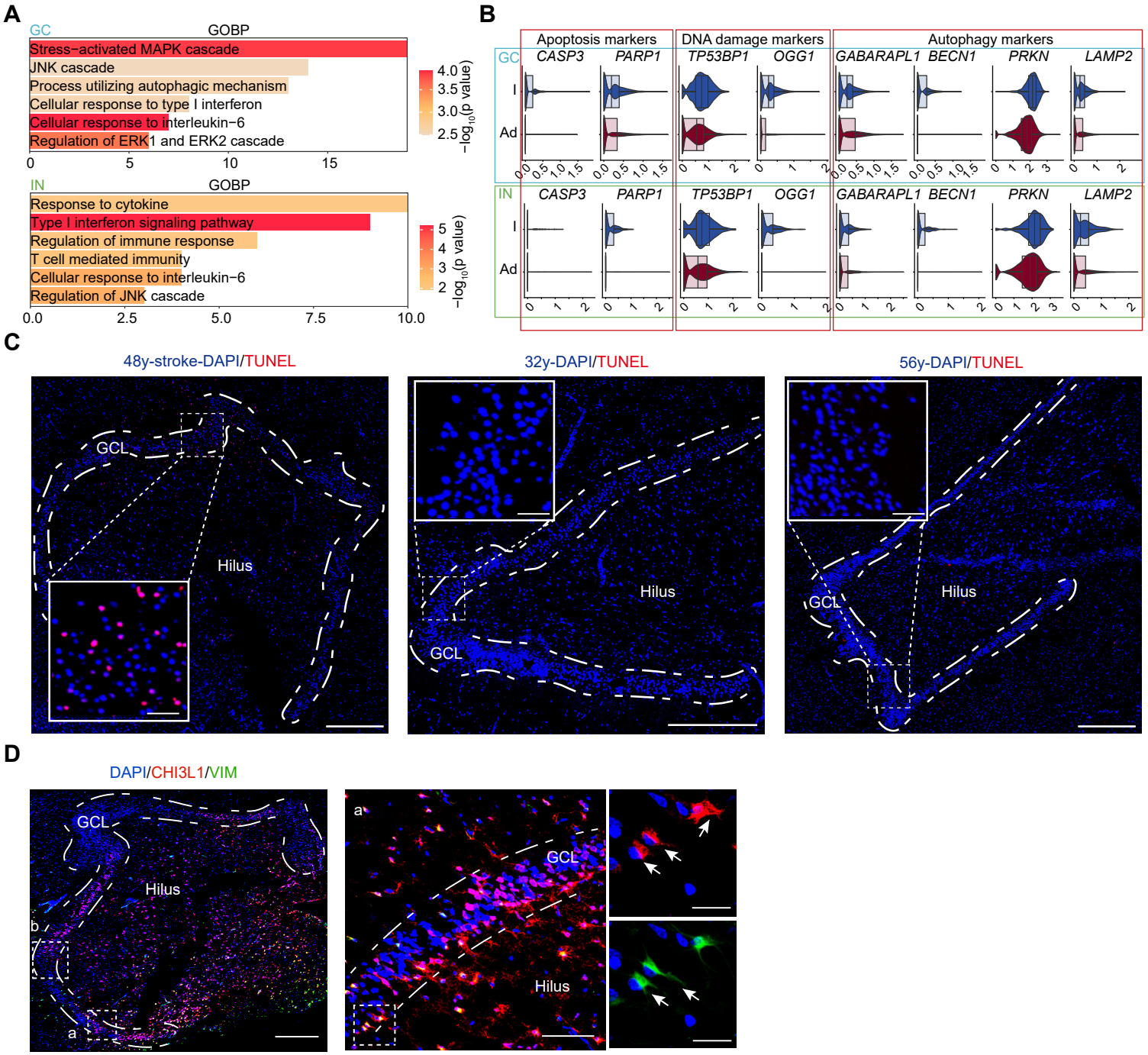
A
GC
GOBP
Stress−activated MAPK cascade
JNK cascade
Process utilizing autophagic mechanism
Cellular response to type I interferon
Cellular response to interleukin−6
Regulation of ERK1 and ERK2 cascade
0
5
10
15
4.0
3.5
3.0
2.5
−log10(p value)
IN
GOBP
Response to cytokine
Type I interferon signaling pathway
Regulation of immune response
T cell mediated immunity
Cellular response to interleukin−6
Regulation of JNK cascade
0.0
2.5
5.0
7.5
10.0
5
4
3
2
−log10(p value)
B
Apoptosis markers
DNA damage markers
Autophagy markers
GC
CASP3
PARP1
TP53BP1
OGG1
GABARAPL1
BECN1
PRKN
LAMP2
I
Ad
IN
CASP3
PARP1
TP53BP1
OGG1
GABARAPL1
BECN1
PRKN
LAMP2
I
Ad
C
48y-stroke-DAPI/TUNEL
GCL
Hilus
32y-DAPI/TUNEL
Hilus
GCL
56y-DAPI/TUNEL
GCL
Hilus
D
DAPI/CHI3L1/VIM
GCL
Hilus
b
a
a
GCL
Hilus

Figure S6

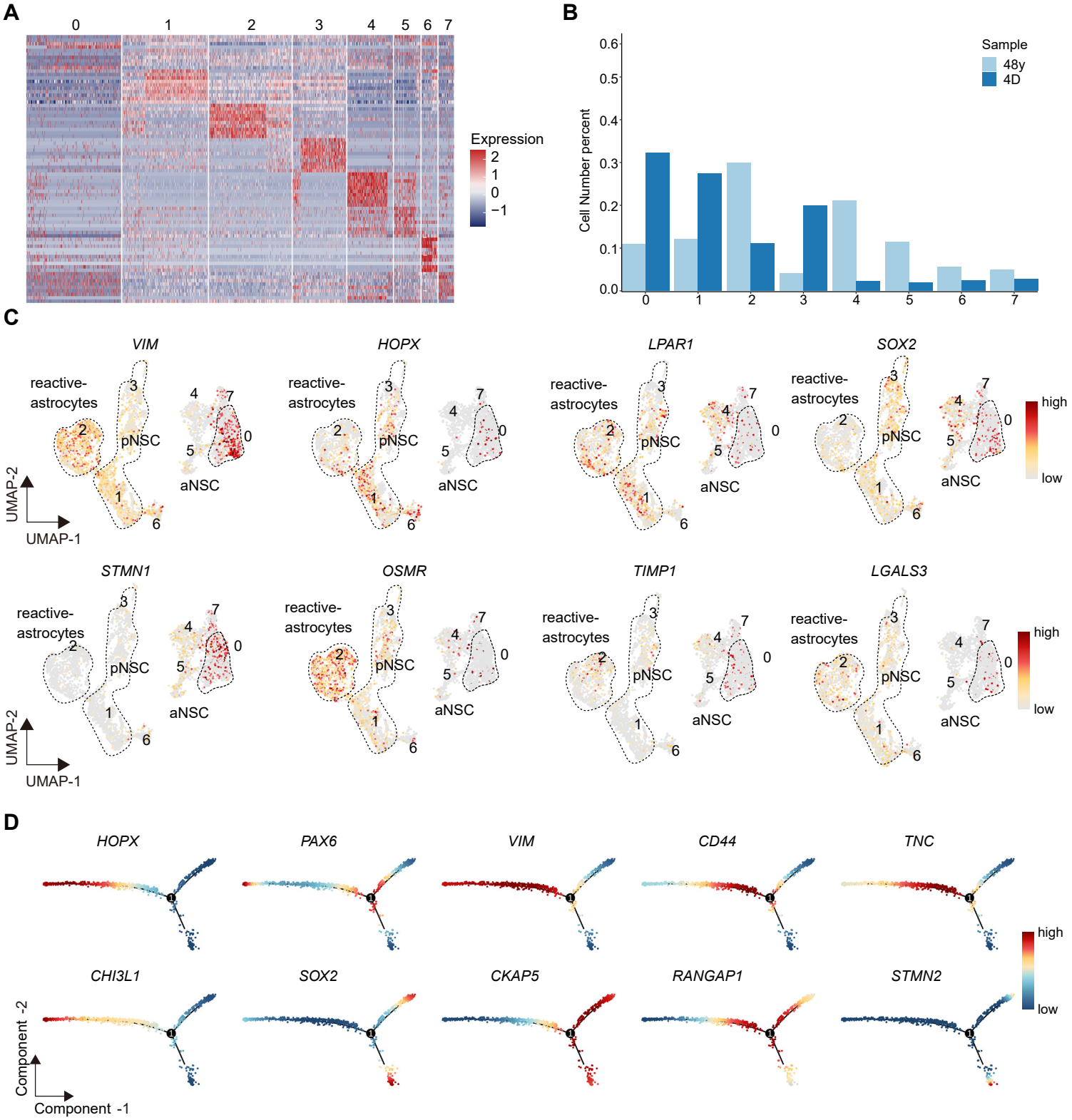
A
0
1
2
3
4
5
6
7
Expression
2
1
0
−1
B
Sample
48y
4D
Cell Number percent
0.6
0.5
0.4
0.3
0.2
0.1
0.0
C
VIM
HOPX
LPAR1
SOX2
STMN1
OSMR
TIMP1
LGALS3
reactive-astrocytes
pNSC
aNSC
UMAP-2
UMAP-1
high
low
D
HOPX
PAX6
VIM
CD44
TNC
CHI3L1
SOX2
CKAP5
RANGAP1
STMN2
Component -2
Component -1

Figure S7

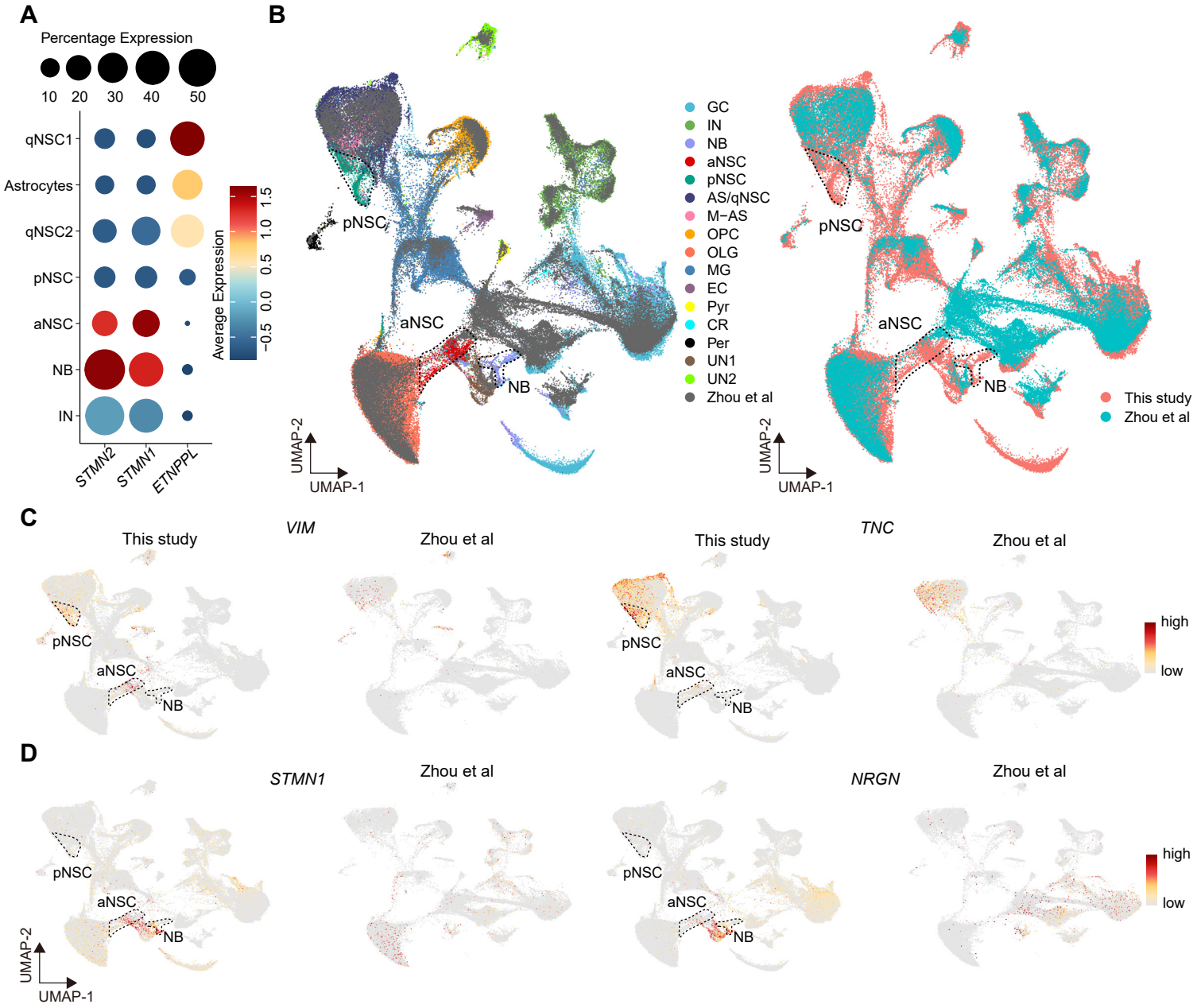
A
Percentage Expression
10 20 30 40 50
qNSC1
Astrocytes
qNSC2
pNSC
aNSC
NB
IN
STMN2
STMN1
ETNPPL
Average Expression
−0.5 0.0 0.5 1.0 1.5
B
pNSC
aNSC
NB
UMAP-2
UMAP-1
GC
IN
NB
aNSC
pNSC
AS/qNSC
M−AS
OPC
OLG
MG
EC
Pyr
CR
Per
UN1
UN2
Zhou et al
This study
Zhou et al
C
This study
VIM
Zhou et al
This study
TNC
Zhou et al
high
low
D
STMN1
Zhou et al
NRGN
Zhou et al
high
low

Figure S8